UNIVERSITI PUTRA MALAYSIA

PREPARATION OF FOOD WASTE - DERIVED BIOCHAR FOR ADSORPTION OF METHYLENE BLUE

ANISAH SAHIMI

PREPARATION OF FOOD WASTE - DERIVED BIOCHAR FOR ADSORPTION OF METHYLENE BLUE

By

ANISAH BINTI SAHIMI

S34110

DEPARTMENT OF SCIENCE AND TECHNOLOGY

FACULTY OF HUMANITIES, MANAGEMENT, AND SCIENCE

UNIVERSITI PUTRA MALAYSIA

2025/2026

PREPARATION OF FOOD WASTE - DERIVED BIOCHAR FOR ADSORPTION OF METHYLENE BLUE

BY

ANISAH BINTI SAHIMI

S34110

PROJECT REPORT SUBMITTED IN PARTIAL FULFILMENT OF THE REQUIREMENT FOR THE DEGREE OF BACHELOR OD SCIENCE IN INDUSTRIAL CHEMISTRY WITH HONOURS ON THE DEPARTMENT OF SCIENCE AND TECHNOLOGY, FACULTY OF HUMANITIES, MANAGEMENT AND SCIENCE,

UNIVERSITI PUTRA MALAYSIA

2025/2026

Abstract of thesis presented to the senate of Universiti Putra Malaysia in fulfilment of the requirement for the degree of Bachelor of Science in Industrial Chemistry with Honours.

PREPARATION OF FOOD WASTE DERIVED BIOCHAR FOR ADSORPTION OF METHYLENE BLUE

By

ANISAH BINTI SAHIMI

March 2026

Chairman : Yiu Pang Hung, PhD

Faculty : Humanities, Management and Science

Food waste-derived biochar (BC) was synthesized from mixed food waste collected from offshore and marine vessels and evaluated for the adsorption of methylene blue (MB) from aqueous solutions. BC was produced by carbonization at 300 °C, 500 °C, and 700 °C. Physicochemical characterization shows that increasing carbonization temperature improves structural stability, surface roughness, and aromaticity. BC prepared at 700 °C exhibits well-developed porosity, enhanced thermal stability, and a heterogeneous carbon matrix, making it the most effective adsorbent among the

prepared samples. Batch adsorption experiments reveal that MB removal is strongly influenced by operating conditions. Adsorption capacity increases with BC dosage, with optimal performance at 50 mg. Solution pH exerts a dominant effect, with maximum removal achieved under alkaline conditions at pH 12.21 due to electrostatic attraction between negatively charged BC surfaces and cationic MB. Temperature enhances adsorption performance, with the highest uptake recorded at 45 °C, indicating an endothermic process. Under optimized conditions, BC achieves an equilibrium adsorption capacity of approximately 47–49 mg/g and removal efficiency exceeding 95% for initial MB concentrations of 5–20 mg/L within 120 min. Kinetic analysis shows that adsorption follows the pseudo-second-order (PSO) kinetic model with high correlation coefficients, confirming chemisorption as the rate-controlling step, while poor agreement with the pseudo-first-order (PFO) kinetic model excludes diffusion-controlled uptake. Regeneration studies demonstrate that BC retains 93.49% removal efficiency in the first cycle and remains above 80% after two cycles, with a gradual decline to 62.83% after four cycles. A bottom-up cost analysis estimates the laboratory-scale production cost at approximately RM 2.07/g, dominated by energy consumption, with negligible raw material cost due to waste-derived feedstock. Overall, MB adsorption onto food waste-derived BC proceeds via synergistic electrostatic attraction, π–π interactions, and hydrogen bonding on a heterogeneous surface. The combination of high adsorption efficiency, moderate regeneration stability, and low production cost highlights food- waste derived BC as a promising, scalable adsorbent for dye-contaminated wastewater treatment.

Keywords: Adsorption; Biochar; Carbonization; Methylene Blue; Wastewater Treatment

Abstrak tesis yang dikemukakan kepada senat Universiti Putra Malaysia sebagai memenuhi keperluan untuk Ijazah Sarjana Muda Sains dalam Kimia Perindustrian dengan Kepujian

Oleh

ANISAH BINTI SAHIMI

MARCH 2026

Pengerusi : **Yiu Pang Hung, PhD**

Fakulti : **Kemanusian, Pengurusan dan Sains**

Kajian ini melaporkan bioarang (BC) yang diperoleh daripada sisa makanan disintesis menggunakan sisa makanan campuran yang dikumpulkan daripada kapal luar pesisir dan marin, dan seterusnya dinilai bagi penjerapan metilena biru (MB) daripada larutan akueus. BC dihasilkan melalui proses pengkarbonan pada suhu 300 °C, 500 °C dan 700 °C. Pencirian fizikokimia menunjukkan bahawa peningkatan suhu pengkarbonan meningkatkan kestabilan struktur, kekasaran permukaan dan tahap keharuman (aromatisiti). BC yang disediakan pada suhu 700 °C menunjukkan keliangan yang berkembang dengan baik, kestabilan terma yang lebih tinggi dan matriks karbon yang heterogen, menjadikannya penjerap paling berkesan dalam kalangan sampel yang disediakan. Eksperimen penjerapan secara kelompok menunjukkan bahawa penyingkiran MB sangat dipengaruhi oleh keadaan operasi. Kapasiti penjerapan meningkat dengan pertambahan dos BC, dengan prestasi optimum dicapai pada dos

50 mg. pH larutan memberikan kesan yang dominan, dengan penyingkiran maksimum diperoleh dalam keadaan beralkali pada pH 12.21, disebabkan oleh tarikan elektrostatik antara permukaan BC bercas negatif dan MB bercas kationik. Peningkatan suhu turut meningkatkan prestasi penjerapan, dengan pengambilan tertinggi direkodkan pada 45 °C, yang menunjukkan bahawa proses ini bersifat endotermik. Di bawah keadaan yang dioptimumkan, BC mencapai kapasiti penjerapan keseimbangan kira-kira 47-49 mg/g dan kecekapan penyingkiran melebihi 95% bagi kepekatan awal MB antara 5–20 mg/L dalam tempoh 120 min. Analisis kinetik menunjukkan bahawa proses penjerapan mengikuti model kinetik pseudo-tertib kedua (PSO) dengan pekali korelasi yang tinggi, sekali gus mengesahkan bahawa penjerapan kimia merupakan langkah pengawal kadar. Sebaliknya, kesepadanan yang lemah dengan model kinetik pseudo-tertib pertama (PFO) menolak mekanisme pengambilan yang dikawal oleh resapan. Kajian penjanaan semula menunjukkan bahawa BC mengekalkan kecekapan penyingkiran sebanyak 93.49% dalam kitaran pertama dan kekal melebihi 80% selepas dua kitaran, dengan penurunan beransur-ansur kepada 62.83% selepas empat kitaran. Analisis kos menggunakan pendekatan bawah ke atas menganggarkan kos pengeluaran pada skala makmal kira-kira RM 2.07/g, yang didominasi oleh penggunaan tenaga, manakala kos bahan mentah adalah minimum kerana sumber bahan mentah berasal daripada sisa. Secara keseluruhan, penjerapan MB ke atas BC yang diperoleh daripada sisa makanan berlaku melalui sinergi tarikan elektrostatik, interaksi π–π dan ikatan hidrogen pada permukaan yang heterogen. Gabungan kecekapan penjerapan yang tinggi, kestabilan penjanaan semula yang sederhana serta kos pengeluaran yang rendah menyerlahkan BC yang diperoleh daripada sisa makanan sebagai penjerap yang berpotensi dan boleh diskalakan untuk aplikasi rawatan air sisa yang tercemar dengan pewarna.

Kata kunci: Penjerapan; Bioarang; Pengkarbonan; Metilena Biru; Rawatan Air Sisa

Graphical Abstract

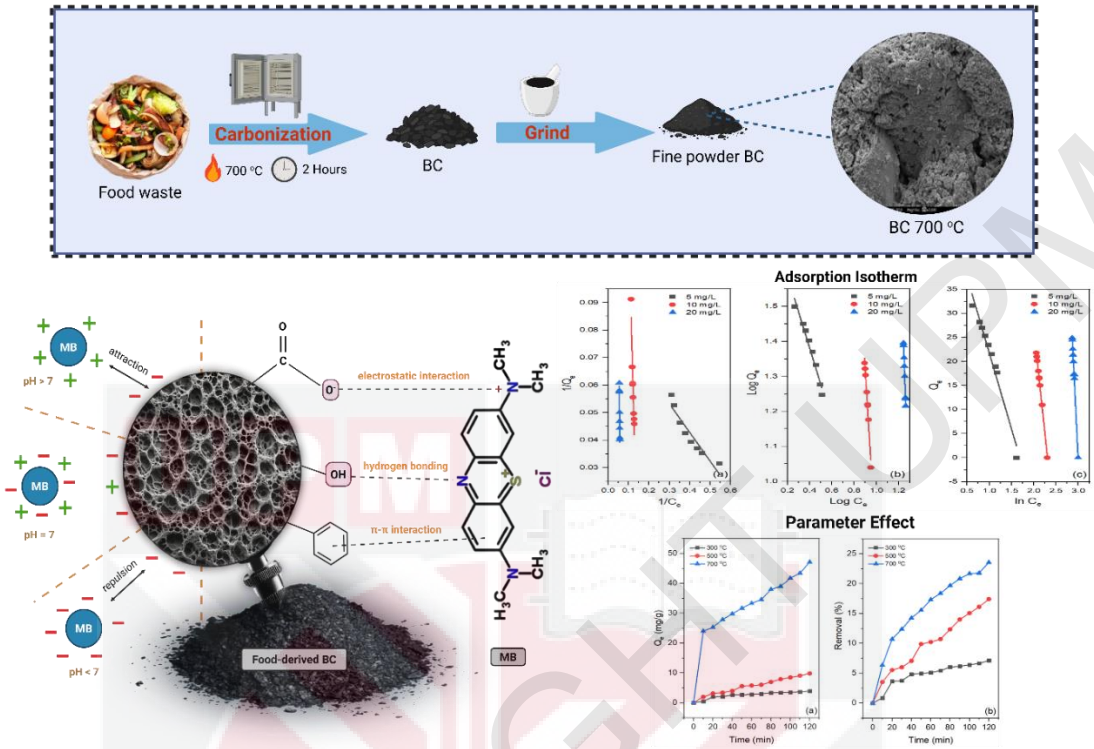

Highlights

- BC700 exhibited well-developed pore structure and abundant surface functional groups, enhancing its adsorption performance toward methylene blue (MB).
- Optimal conditions for MB adsorption, including an adsorbent dosage of 50 mg, a basic pH of 12.21, low MB concentration of 5 mg/L, at 45 °C within 120 minutes.
- Adsorption kinetics followed the Elovich model at low concentration and PSO model at higher concentration, while isotherm followed the Temkin model.
- BC700 demonstrated high adsorption capacity and removal efficiency, highlighting its potential as a low-cost and sustainable adsorbent for wastewater treatment.

ACKNOWLEDGEMENT

In the name of Allah, the Most Merciful and the Most Compassionate.

There were many moments in this journey when I felt that I was not enough. I struggled with understanding, with confidence, and with fear of failure. At times, I questioned my own ability to complete this research. Yet, through every hardship, Allah granted me patience, strength, and the presence of people who never gave up on me. For that, I am deeply grateful. This work was made possible not by my effort alone, but by the collective support and sincerity of many individuals who believed in me even when I doubted myself.

I would like to express my sincere appreciation to my supervisor, Assoc. Prof. Dr. Yiu Pang Hung, for his guidance, patience, and constructive feedback throughout this research. His academic direction and insights were invaluable in shaping the framework and direction of this study.

My deepest and most heartfelt gratitude is dedicated to my co-supervisor, Dr. Alvin Lim Teik Zheng. His unwavering support, patience, and dedication played a crucial role in the completion of this research. At times when I felt lost and uncertain, he provided clarity; when I felt incapable, he offered encouragement. His willingness to devote time and effort to guide me, even beyond academic expectations, gave me the confidence to continue. I am profoundly grateful for his mentorship, which has greatly contributed not only to this project but also to my personal and academic growth.

I would also like to extend my heartfelt thanks to the laboratory assistants, Cik Khairunnisa and Encik Syafiran, for their invaluable assistance throughout this project. Their guidance in handling laboratory instruments allowed me to gain confidence and accuracy in conducting my experiments. As someone who was often uncertain and

afraid of making mistakes, their patience and willingness to teach were a great source of comfort and motivation.

Behind every achievement lies silent sacrifices. To my family, I owe more than words can express. They witnessed my frustration, my exhaustion, and my tears, yet they never stopped believing in me. Their prayers and encouragement became my strength when I felt that I had none left. Even when I doubted myself, they never doubted me.

To my friends, Nadya and Chai, thank you for your encouragement and willingness to help me throughout this journey. Your support, whether through words or actions, gave me strength during moments when I felt exhausted and uncertain. My deepest gratitude goes especially to Syakirah. Throughout this project, she was not only a friend, but also a source of guidance and reassurance. There were many times when I felt lost and incapable, yet she patiently explained, taught, and guided me without ever making me feel small. Her patience, kindness, and constant willingness to help carried me through moments when I felt close to giving up. I am profoundly grateful for her sincerity and the quiet sacrifices she made to support me along this journey.

Last but not least, I would like to acknowledge myself. I am thankful not because I was brilliant, but because I did not give up. I am grateful for the courage to continue even when I felt inadequate, for the patience to endure repeated failures, and for the heart that remained soft despite the pressure of this journey. This experience has taught me that success is not always born from intelligence, but often from perseverance, faith, and the kindness of those who walk beside us.

PREPARATION OF FOOD WASTE – DERIVED BIOCHAR FOR ADSORPTION OF METHYLENE BLUE

BY

ANISAH BINTI SAHIMI

S34110

APPROVED BY

Supervisor

_____ Date: 29th March 2026

(ASSOC. PROF. DR YIU PANG HUNG)

Project Coordinator

DR. SIVASANGAR SEENIVASAGAM
Pensyarah Kanan
Jabatan Sains dan Teknologi
Fakulti Kemanusiaan, Pengurusan dan Sains
Universiti Putra Malaysia Kampus Bintulu Sarawak

Date: 6 / 4 / 2026

(DR. SIVASANGAR SEENIVASAGAM)

TABLE OF CONTENTS

LIST OF TABLES

LIST OF FIGURES

LIST OF ABBREVIATIONS

AC	Activated carbon
BC	Biochar
FESEM	Field emission scanning electron microscopy
FTIR	Fourier transform infrared spectroscopy
IPD	Intraparticle diffusion
MB	Methylene blue
PFO	Pseudo-first-order
PSO	Pseudo-second-order
TGA	Thermogravimetric analysis
XRD	X-ray diffraction

CHAPTER 1

INTRODUCTION

1.1 General background

Water pollution remains a critical environmental challenge due to the continuous discharge of industrial effluents into natural water bodies. Among various classes of contaminants, synthetic dyes represent a major concern because of their high visibility, chemical stability, and resistance to biodegradation. Industries such as textiles, leather processing, paper manufacturing, and plastics release large volumes of dye-laden wastewater, which significantly degrades water quality and aquatic ecosystems (Periyasamy, 2024).

Methylene blue (MB) is one of the most widely used cationic dyes in industrial applications. Its extensive use, coupled with incomplete removal during conventional wastewater treatment, leads to frequent detection in surface and groundwater. Exposure to MB-contaminated water has been associated with adverse ecological effects and potential health risks, including irritation, toxicity to aquatic organisms, and disruption of photosynthetic processes (Khan et al., 2022). These concerns have intensified the demand for effective, economical, and environmentally sustainable treatment strategies.

Conventional dye removal methods, including chemical oxidation, coagulation–flocculation, membrane filtration, and biological treatment, suffer from notable limitations. These include high operational costs, complex process control, energy-intensive operation, and the generation of secondary pollutants such as sludge. As a result, adsorption has emerged as a preferred treatment technique due to its operational simplicity, flexibility, and high removal efficiency for a wide range of organic pollutants (Chatzimichailidou et al., 2023; Satyam & Patra, 2024).

Activated carbon (AC) is widely recognized as an effective adsorbent for dye removal. Nevertheless, its high production cost and reliance on non-renewable precursors restrict large-scale application, particularly in developing regions. This limitation has driven growing research interest in low-cost, biomass-derived carbon materials as sustainable alternatives for dye removal (Dong et al., 2024; Z. Li et al., 2023; Xie et al., 2022). In this context, BC derived from waste biomass has gained increasing attention. BC is a carbon-rich material produced through the thermal decomposition of organic feedstocks under oxygen-limited conditions. Its surface functional groups, porosity, and physicochemical properties can be tailored through controlled preparation conditions, making it suitable for adsorption applications (Manyà, 2012). Importantly, BC production supports waste valorization and aligns with circular economy principles by converting organic waste into value-added functional materials.

Food waste represents an abundant and underutilized biomass resource. The disposal of food waste contributes to greenhouse gas emissions and landfill overcapacity (Moureen et al., 2024). Transforming food waste into BC offers a dual environmental benefit by addressing waste management challenges while producing a functional adsorbent for water treatment (Handayati & Widyanata, 2024). Despite this potential, systematic studies on food waste-derived BC for dye adsorption remain limited compared to agricultural and lignocellulosic residues.

1.2 Problem statement

Despite extensive research on dye removal technologies, several unresolved challenges persist in the treatment of MB-contaminated wastewater. First, MB exhibits high chemical stability and strong coloration even at low concentrations, making its removal from aqueous systems technically demanding (Khan et al., 2022). Conventional treatment processes often fail to achieve complete removal or require high energy input and chemical consumption. Second, while adsorption using

commercial AC demonstrates high efficiency, its widespread application is constrained by high cost, regeneration difficulty, and sustainability concerns. The dependence on fossil-based or high-value precursors further limits its suitability for long-term wastewater treatment strategies. Third, although biomass-derived BC has emerged as a promising alternative adsorbent, most existing studies focus on agricultural residues such as rice husk, sawdust, or fruit peels (Ahmad et al., 2020; Z. Li et al., 2023; Olupot et al., 2024; Ortega-Toro et al., 2023; Sahu et al., 2020; Tolkou et al., 2024). Food waste-derived BC remains comparatively underexplored, particularly in relation to systematic optimization of carbonization temperature, surface chemistry, adsorption kinetics, and thermodynamic behavior. Finally, many reported studies emphasize adsorption capacity alone, without integrating regeneration performance and cost considerations. This limits the practical assessment of BC for real-world wastewater treatment applications. These gaps highlight the need for a comprehensive investigation into food waste-derived BC as a sustainable adsorbent for MB removal, incorporating performance evaluation, mechanistic understanding, and economic feasibility.

1.3 Research gap

A critical review of existing literature reveals several specific gaps. First, there is limited systematic research on BC synthesized from food waste feedstocks, particularly with respect to the influence of carbonization temperature on surface functionality, porosity development, and adsorption behavior. Second, the adsorption mechanisms governing MB uptake by food waste-derived BC remain insufficiently elucidated. Many studies report kinetic and isotherm models without critically linking them to surface chemistry and adsorption pathways. Third, regeneration and reusability studies are often omitted or treated as secondary considerations, despite their importance for sustainable application. Fourth, few studies integrate adsorption performance with cost analysis, which is essential for evaluating scalability and industrial relevance.

Addressing these gaps is necessary to advance the scientific understanding and practical deployment of food waste-derived BC in wastewater treatment.

1.4 Research objectives

The overall objective of this study is to evaluate the feasibility of food waste-derived BC as an efficient and sustainable adsorbent for MB removal from aqueous solutions.

The specific objectives are:

i. To prepare and characterize BC from food waste-derived waste.
ii. To investigate the adsorption efficiency of the prepared BC for MB removal under varying operational parameters.
iii. To analyze the adsorption behavior using kinetic and isotherm models.
iv. To assess the economic feasibility of the food waste-derived BC by estimating preparation cost relative to adsorption performance.

1.5 Significance of the study

This study provides original experimental insight into the conversion of food waste into functional BC for wastewater treatment applications. By systematically linking synthesis conditions, material properties, adsorption performance, and regeneration behavior, the work advances mechanistic understanding of MB adsorption on food waste-derived BC. From an environmental perspective, the study supports sustainable waste management through food waste valorization while addressing dye pollution in aquatic systems. From a practical standpoint, the integration of performance evaluation with cost analysis enhances the relevance of the findings for real-world implementation. Overall, this research contributes to the development of low-cost, sustainable adsorbents and supports broader efforts toward circular economy-driven water treatment solutions.

CHAPTER 2

LITERATURE REVIEW

2.1 Food waste as a sustainable precursor for BC production

Food waste represents a major global sustainability challenge, with approximately one-third of all food produced worldwide, around 1.3 billion tons annually, being lost or discarded across the supply chain (Kumari et al., 2024). Such waste contributes substantially to greenhouse gas emissions, landfill saturation, and inefficient resource utilization (Scherhaufer et al., 2018). Against this backdrop, the conversion of food waste into value-added materials has emerged as a key strategy within circular economy frameworks.

Among available valorization routes, the transformation of food waste into BC through thermal treatment offers a particularly attractive pathway. Food waste-derived BC converts heterogeneous organic waste into a stable carbonaceous material with applications in environmental remediation and agriculture (Zakaria et al., 2023). Carbonization or pyrolysis of food waste simultaneously addresses waste management challenges while generating functional materials capable of pollutant removal (Haris et al., 2021; Shanmugam et al., 2024; Y. Shao et al., 2023a).

The properties of food waste-derived BC are strongly governed by feedstock composition and carbonization parameters. Thermal decomposition in oxygen-limited environments, typically between 300 and 700 °C, produces BC with variable surface area, porosity, and functional group distribution. Pretreatment strategies such as torrefaction or hydrothermal carbonization further influence elemental ratios, hydrophobicity, and adsorption-relevant characteristics (W.-H. Chen et al., 2021; Kim et al., 2015; Krysanova et al., 2022). These findings highlight both the opportunity and complexity associated with heterogeneous food waste feedstocks.

2.2 Carbonization processes and structure–property relationships

Carbonization is the central step governing BC formation and functionality. During thermal treatment, dehydration, devolatilization, and carbon rearrangement progressively transform biomass into a carbon-rich solid (Kujawska & Wasag, 2021). Carbonization temperature critically influences BC structure. Lower temperatures favor retention of oxygenated functional groups and amorphous carbon, while higher temperatures enhance aromatization, pore development, and thermal stability (Hou et al., 2024). One previous study report that increasing carbonization temperature within the 300–700 °C range improves microporosity and adsorption performance for organic contaminants (Kuang et al., 2020). However, higher temperatures also reduce yield and increase ash content, highlighting the need for balanced optimization, particularly for heterogeneous food waste feedstocks. Textural evolution is particularly critical for adsorption performance. Previous study has shown that higher carbonization temperatures strongly promote micropore formation, with micropore volume and surface area increasing steadily as temperature rises from 400 °C to 900 °C (Řimnáčová et al., 2024). CO_2 and N_2 sorption analyses confirmed that adsorption capacity correlates positively with micropore volume, as narrow micropores provide high-energy adsorption sites through preferential pore filling. Raman spectroscopy further supported this trend by revealing increasing aromatic ordering and polyaromatic clustering at higher temperatures, which contributes to the development of a stable microporous network.

At lower carbonization temperatures, BC retains a higher proportion of oxygen-containing functional groups and amorphous carbon domains. Liu et al. demonstrated that BCs produced from crop residues at 300-400 °C exhibit higher H/C and O/C ratios, reflecting incomplete deoxygenation and lower aromatic condensation (Liu et al., 2018). FTIR and elemental analyses in that work showed pronounced –OH and –

COOH functionalities at lower temperatures, which progressively diminish as temperature increases due to dehydration and decarboxylation reactions. These surface functionalities enhance hydrophilicity and surface polarity but limit thermal stability and structural ordering. As carbonization temperature increases, pronounced changes in textural and structural properties occur. Lu et al. (2022a) reported a consistent decrease in volatile matter and a corresponding increase in fixed carbon content between 300 °C and 600 °C, accompanied by a reduction in H/C and O/C ratios. These trends indicate increasing aromatization and the formation of condensed carbon structures. SEM images revealed progressive pore development from original plant cell walls, while XRD patterns showed the evolution from largely amorphous carbon toward turbostratic carbon structures at higher temperatures.

2.3 MB as a model cationic dye pollutant

MB is a cationic dye frequently used as a model pollutant in wastewater treatment research due to its widespread industrial application and environmental concerns. The physicochemical properties of MB are summarized in Table 2.1. Its removal from aqueous solutions is a significant area of focus, primarily through adsorption processes utilizing a diverse range of materials and methodologies (Takele et al., 2025). MB dye finds extensive use in various industrial applications, including textile dyeing, paper colouring, and as a biological stain in laboratories. Its widespread application, particularly in the textile industry, leads to significant environmental concerns due to its discharge into wastewater.

Table 2.1. The structure and properties of MB.

Chemical Structure	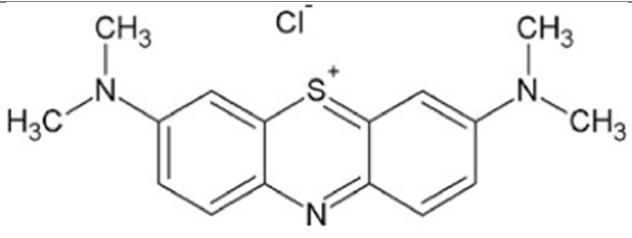

Chemical formula	$C_{16}H_{18}ClN_3S$
Colour	Dark green crystals or powder with a bronze-like luster; Solutions in water or alcohol are deep blue.
Melting point	100 to 110 °C (with decomposition)
Molecular weight	319.9 g/mol
Solubility	Highly soluble in water and polar organic solvents such as ethanol and chloroform
Stability/Shelf life	Stable under recommended storage conditions.
Vapor pressure	0.00000013 [mmHg]

The environmental impact of MB is substantial because it is a synthetic organic dye known for its high resistance to biodegradation. When released into aquatic environments, MB can cause several detrimental effects. It imparts an undesirable colour to water bodies, reducing light penetration and consequently hindering photosynthetic activity of aquatic plants and algae. This disruption to primary producers can cascade through the aquatic food web, affecting oxygen levels and overall ecosystem health. Furthermore, MB and its degradation products can be toxic to aquatic organisms and potentially to humans through the consumption of contaminated water or bioaccumulation in the food chain. The aesthetic pollution caused by coloured wastewater also negatively impacts the recreational value of water resources and can harm the public perception of environmental quality (Takele et al., 2025).

2.4 Adsorptive performance of food waste-derived BC for MB removal

Food waste-derived BC has been widely reported as an effective adsorbent for MB removal from aqueous systems. Existing studies show that adsorption performance

depends strongly on the nature of the food waste precursor, carbonization temperature, and resulting surface chemistry, which together regulate pore development, aromaticity, and the distribution of surface functional groups. BC produced from fruit and food wastes has demonstrated promising MB adsorption under optimized preparation conditions. For example, jackfruit peel-derived BC carbonized at 500 °C possessed maximum adsorption capacity of 38.5 mg/g (Loc Ton-That et al., 2023). The observed performance was linked to oxygen-containing functional groups that enhanced electrostatic attraction between cationic MB molecules and negatively charged BC surfaces. This study highlighted the importance of surface polarity and functional group composition in governing dye uptake.

Similarly, Zamri et al. (2019) synthesized banana peel BC via carbonization at 400 °C and achieved a maximum MB removal efficiency of approximately 99% under optimal conditions. The adsorption mechanism was dominated by electrostatic attraction and surface complexation involving hydroxyl and carboxyl functional groups. The authors highlighted the practical advantages of fruit waste-based BC, particularly its abundance and low production cost, which make it suitable for small-scale wastewater treatment applications.

Beyond dye adsorption, food waste-derived BC has also been investigated for contaminant removal more broadly, offering insight into structure-performance relationships. Moureen et al. (2024) converted food waste into BC through pyrolysis at temperatures between 350 °C and 550 °C and evaluated its physicochemical properties and adsorption behavior. Increasing pyrolysis temperature reduced BC yield while increasing ash content and alkalinity, with BC produced at 550 °C exhibiting the highest removal efficiency for selected contaminants. The enhanced adsorption was attributed to increased alkalinity, negatively charged surface sites, and oxygen-containing functional groups. Equilibrium data followed the Freundlich isotherm, indicating heterogeneous surface adsorption, and optimal performance was achieved

at pH 8 with a contact time of 120 min. The role of carbonization temperature has been further highlighted in studies using coconut-based feedstocks. Musa et al. (2025) reported enhanced MB adsorption performance for coconut husk BC prepared at higher carbonization temperatures. In their work, BC produced at 600 °C showed the highest adsorption capacity, with the pristine sample (CSB600) exhibiting a capacity of 5.590 mg/g. The improved performance was attributed to increased aromaticity and the development of a microporous surface structure. The study concluded that optimizing carbonization temperature is critical for enhancing adsorption performance, as higher temperatures promote the formation of stable, graphitic carbon structures that interact effectively with cationic dye molecules, while magnetisation had no significant influence on adsorption capacity.

Adsorption kinetics for MB on food waste-derived BCs are frequently well described by the pseudo-second-order (PSO) model, as demonstrated in multiple studies (J. Wang et al., 2023).This implies that the rate-limiting step is chemical adsorption involving electron sharing or exchange between adsorbent and adsorbate. Common isotherm models used to describe adsorption equilibrium include Langmuir, Freundlich, Sips, and Dubinin-Radushkevich (Loc Ton-That et al., 2023; J. Wang et al., 2023). For example, the adsorption data for jackfruit peel BC best fit the Sips and Freundlich models, suggesting heterogeneous surface adsorption. In contrast, the Langmuir isotherm model was most suitable for describing the adsorption equilibrium of $Ca(OH)_2$-modified rice straw BC and eggshell membrane-derived BC, indicating monolayer adsorption on uniform sites.

Several key factors influence the adsorption efficiency of MB onto BC. The solution pH is critical because it affects both the surface charge of BC and the ionization state of MB, thereby modifying electrostatic interactions between the adsorbent and adsorbate (Loc Ton-That et al., 2023). Contact time also plays a significant role; adsorption capacity typically increases with time until equilibrium is established, at which point no

further adsorption occurs. The initial concentration of MB impacts the adsorption capacity as well, with higher concentrations generally leading to greater uptake until the saturation point of adsorption sites is reached. Moreover, the dosage of BC used directly affects the availability of adsorption sites, influencing the overall removal efficiency (El Jery et al., 2024).Temperature can further affect the kinetics and thermodynamics of the adsorption process, altering both the rate and extent of MB uptake (El Jery et al., 2024).

Studies using untreated food residues further demonstrate the adsorption potential of food waste-derived materials. Tolkou et al. (2024) investigated banana, orange, and pomegranate peels as natural adsorbents for both anionic and cationic dyes, including MB. High MB removal efficiency, up to 98%, was achieved at alkaline pH, with adsorption kinetics better described by the PSO model. Freundlich and Langmuir isotherms were both applicable depending on the system, reflecting surface heterogeneity. The materials retained appreciable adsorption capacity over multiple reuse cycles, supporting the practical viability of food waste-based adsorbents.

Recent advances have also focused on understanding the molecular structure of food waste–derived BC to elucidate adsorption mechanisms. Qing et al. (2024) combined experimental characterization and quantum chemical modelling to investigate BC prepared from food waste pyrolysis. Their results showed that BC produced at intermediate temperatures, particularly around 450 °C, retained diverse oxygen- and nitrogen-containing functional groups that served as effective adsorption sites. Functional groups such as carboxyl, carbonyl, hydroxyl, and amine moieties were identified as key contributors to adsorption through electrostatic interactions and surface complexation, providing mechanistic insight into pollutant uptake.

2.5 Mechanisms governing MB adsorption onto BC

MB adsorption onto BC involves multiple, simultaneous mechanisms. Electrostatic attraction plays a dominant role due to the cationic nature of MB and the pH-dependent surface charge of BC (El Jery et al., 2024). Pore filling within micro- and mesopores contributes to physical entrapment, while hydrogen bonding strengthens interactions with polar surface groups. (Gayathiri et al., 2023; G.P. Avinash et al., 2025). π–π stacking between aromatic MB molecules and graphitic BC domains further enhances adsorption, particularly at higher carbonization temperatures. Surface complexation involving functional groups contributes to stronger, more stable adsorption, especially in chemically modified BC systems (Meftah et al., 2024). Recent molecular-level studies confirm the critical role of oxygen- and nitrogen-containing functional groups in defining adsorption sites and interaction strength

For instance, in the case of cattle manure BC, ash-related effects introduce additional adsorption pathways that reinforce these mechanisms. Under alkaline conditions, negatively charged surface species derived from ash, including phosphate and silicate groups, increase surface charge density and strengthen electrostatic attraction toward MB. Cation exchange also contributes through the substitution of exchangeable inorganic cations such as Ca^{2+}, Mg^{2+}, Na^{+}, K^{+}, and H^{+} by MB molecules. Hydrogen bonding remains active through surface oxygen functionalities, while aromatic regions facilitate both π–π and n–π interactions with MB. Physical adsorption and partitioning into noncarbonized fractions occur at sites associated with residual organic matter. As pyrolysis temperature increases, the formation of stable P-Ca-Mg crystalline phases reduce the availability of reactive ash species, leading to weaker electrostatic interactions and diminished ion-exchange capacity. The combined adsorption pathways governing MB uptake on BC are illustrated in Fig. 2.1.

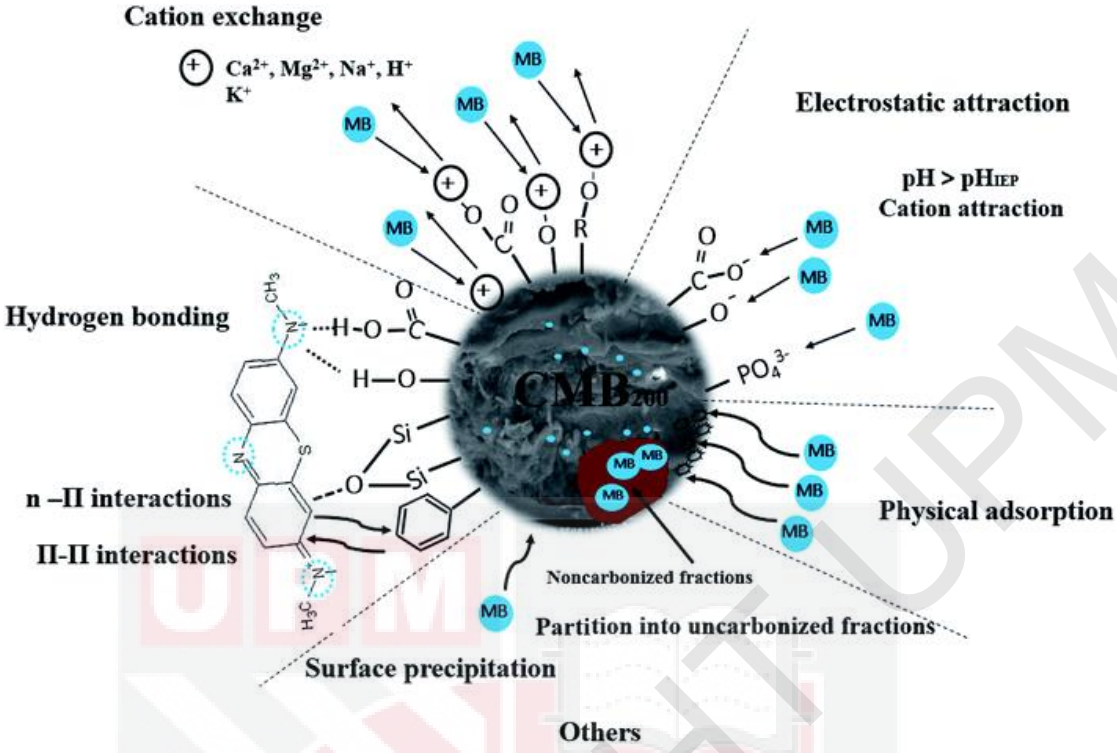

Fig. 2.1. Interaction mechanism of MB on cattle manure BC-MB (Zhu et al., 2018).

2.6 Research gaps and motivation for the present study

Despite extensive research on food waste-derived BC for dye removal, several critical gaps remain:

i. Limited focus on mixed food waste feedstocks: Most studies investigate single, well-defined food wastes such as fruit peels or agricultural residues. The adsorption behavior and reproducibility of BC derived from heterogeneous mixed food waste streams remain underexplored.

ii. Insufficient linkage between carbonization temperature, structure, and adsorption mechanism: While carbonization temperature is known to influence adsorption performance, few studies systematically correlate temperature-driven structural evolution with kinetic, isotherm, and mechanistic behavior for MB adsorption.

iii. Overreliance on chemically activated BCs: Many high-performance systems rely on chemical activation, increasing cost and environmental burden. There is a lack of comprehensive evaluation of unmodified food waste-derived BC produced under mild conditions.

iv. Limited integration of adsorption performance with cost considerations: Adsorption efficiency is often reported without parallel assessment of production cost, limiting practical applicability and scalability evaluation.

v. Incomplete mechanistic validation: Although electrostatic, π–π, and hydrogen-bonding mechanisms are frequently proposed, few studies integrate surface characterization, kinetic modeling, and adsorption behavior into a unified mechanistic framework.

Accordingly, the present study addresses these gaps by systematically converting mixed food waste into BC under controlled carbonization conditions, correlating physicochemical characteristics with MB adsorption performance, elucidating adsorption mechanisms using kinetic and isotherm analyses, and evaluating cost feasibility to assess practical applicability.

CHAPTER 3

MATERIALS AND METHODS

3.1 Materials

Mixed food waste, comprising heterogeneous and non-segregated organic residues of unknown specific origin were collected from offshore and marine vessels. Methylene blue (MB) (Bendosen, Malaysia) was selected as the model pollutant for adsorption studies. Hydrochloric acid, HCl, and sodium hydroxide, NaOH (Merck, Germany), were used for pH adjustment. Ultrapure water with pH 6.5 to 7.0 was used for all solution preparations. All chemicals were of analytical grade and were used without further purification.

3.2 Synthesis of food waste-derived BC

As shown in Fig. 3.1, the obtained food waste was oven-dried to constant mass, manually crushed, and sieved to obtain a uniform particle size suitable for thermal processing. A fixed mass of 10.00 g of the prepared feedstock was transferred into a ceramic crucible and placed in a muffle furnace. Carbonization was conducted at 300 °C, 500 °C, and 700 °C using a constant heating rate of 10 °C per minute. Each target temperature was maintained for 2 h to promote carbon framework development. After the holding period, the furnace was switched off and allowed to cool naturally to room temperature under static conditions to limit oxidative exposure. The resulting BC was collected, lightly ground into a fine powder, and stored in airtight containers to prevent moisture uptake and contamination. These BC samples were used for subsequent adsorption experiments and physicochemical characterization.

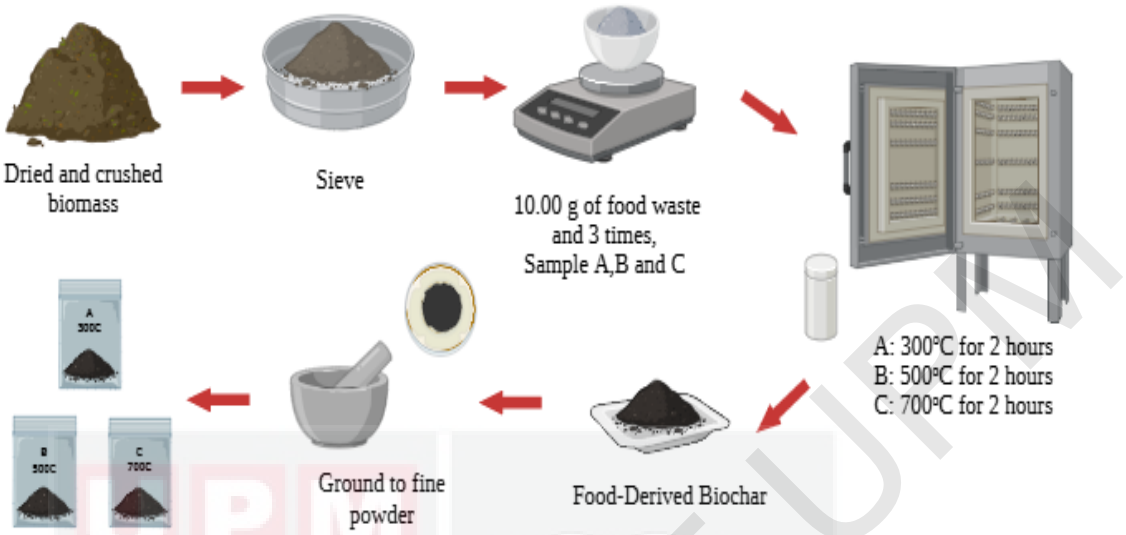

Fig. 3.1. Schematic illustration of the preparation process of food waste-derived BC.

3.3 Characterizations

3.3.1 Chemical characterization – FTIR

Fourier transform infrared (FTIR) spectroscopy was used to identify surface functional groups on food waste-derived BC. Measurements were performed using an Agilent Cary 630 FTIR spectrometer (Agilent Technologies, USA). BC powder was prepared using the KBr pellet method. Approximately 1 mg of BC was homogenized with 100 mg of spectroscopic-grade KBr and ground thoroughly in an agate mortar to ensure uniform mixing. The mixture was compressed into a transparent pellet under 3.5 tons for 15 s. Spectra were recorded in the range of 4000 to 400 cm^{-1} at a resolution of 4 cm^{-1}, with 32 scans averaged per sample. A background spectrum obtained from a blank KBr pellet was subtracted to remove matrix interference. The spectra were interpreted to determine surface functional groups and to evaluate chemical changes induced by the BC preparation process.

3.3.2 Structural characterization – XRD

Powder X-ray diffraction (XRD) analysis was performed to evaluate the structural nature of food waste-derived BC. Samples were finely ground to ensure uniform particle size and evenly packed into the sample holder to obtain a smooth surface and reduce diffraction artifacts. Measurements were conducted using a Shimadzu XRD-6000 powder X-ray diffractometer/ Cu Kα radiation with a wavelength of 1.54056 Å was used. The instrument was operated at 60 kV and 60 mA. Diffraction patterns were recorded over a 2θ range of 5° to 80° with a step size of 0.02° s^{-1}. The XRD patterns were analyzed to confirm the predominantly amorphous structure of BC, characterized by broad and diffuse diffraction features rather than sharp crystalline peaks. This analysis was used to assess structural evolution induced by carbonization temperature.

3.3.3 Morphological characterization – FESEM

The surface morphology of food waste-derived BC was examined using a JEOL JSM-6390 Field-emission Scanning Electron Microscope (FESEM). FESEM analysis provided information on surface texture, pore development, and morphological features relevant to adsorption behavior. Prior to imaging, samples were coated with a thin carbon layer using a HITACHI E-1045 ion sputtering device for 1 min to improve electrical conductivity. Imaging was performed at an accelerating voltage of 5 kV with a magnification of 2000-5000×, enabling clear observation of surface roughness and pore structures formed during the pyrolysis process.

3.3.4 Thermal characterization – TGA

Thermogravimetric (TGA) analysis was performed to evaluate the thermal stability of food waste-derived BC using a Mettler Toledo thermogravimetric analyzer. Measurements were conducted under a nitrogen atmosphere at a flow rate of 100 mL/min to suppress oxidative reactions. The sample was heated from 25 °C to 1000

°C at a constant rate of 10 °C/min. Mass loss and thermal events were analyzed to assess decomposition behavior, thermal stability, and residual ash content. These data provided insight into the fixed carbon fraction and structural robustness of BC relevant to its application as an adsorbent in aqueous systems.

3.4 Adsorption test

A known mass of BC powder was dispersed in 100 mL of an aqueous MB solution with an initial concentration of 10 mg/L. During each adsorption run, 1 mL aliquots were withdrawn at predetermined time intervals and centrifuged at 4000 rpm for 10 min to separate suspended BC prior to analysis. The residual MB concentration was quantified using a calibration curve constructed from standard MB solutions measured at 664 nm. The equilibrium adsorption capacity, Q_e, was calculated using Eq. (3.1).

$$Q_e = \left(\frac{C_0 - C_t}{m}\right) x\, V$$

The percentage removal efficiency was calculated using Eq. (3.2):

$$\%\, removal = \left(\frac{C_0 - C_t}{C_0}\right) x\, 100$$

where C_0 is the initial concentration of MB (mg/L), C_t is the concentration at a specific time (mg/L), V is the volume of the MB solution (L), and m is the mass of the adsorbent (mg).

3.4.1 Comparison of adsorbents

A comparative adsorption study was performed to evaluate the performance of food waste-derived BC prepared at different carbonization temperatures. This comparison was designed to clarify the influence of carbonization temperature on physicochemical properties and adsorption efficiency for MB removal.

3.4.2 Influence pH

The solution pH was adjusted using 0.1 M NaOH for basic conditions and 0.1 M HCl for acidic conditions. pH plays a critical role in adsorption because it governs the surface charge of BC and the ionization state of MB. Changes in pH therefore alter electrostatic interactions between the adsorbent and MB molecules, leading to measurable differences in adsorption efficiency, as reported in previous study (Loc Ton-That et al., 2023).

3.4.3 Influence initial MB concentration

MB solutions with initial concentrations of 5 mg/L, 10 mg/L, and 20 mg/L were prepared to examine the effect of concentration on adsorption behavior. Variation in initial MB concentration affects adsorption by altering the mass transfer driving force between the solution and BC surface. Higher concentrations increase this driving force and generally enhance adsorption capacity until active sites approach saturation. Once site saturation occurs, further increases in MB concentration no longer improve removal efficiency and can reduce the apparent adsorption rate. Similar trends have been reported for food waste-derived BC systems, where elevated dye concentrations lead to site saturation and slower adsorption kinetics (Loc Ton-That et al., 2023).

3.4.4 Influence of adsorbent dosage

The effect of BC dosage on MB adsorption was evaluated using 10 mg, 20 mg, and 50 mg of food waste-derived BC. Increasing the adsorbent dosage increases the number of available adsorption sites, which improves overall MB removal. At higher dosages, particle aggregation and site overlap can occur, reducing the effective surface area and limiting contact between MB molecules and the BC surface. This effect constrains further gains in adsorption efficiency beyond an optimal BC dosage.

3.4.5 Influence of solution temperature

The effect of solution temperature on MB adsorption was investigated at 25 °C, 35 °C, and 45 °C. An increase in temperature led to higher adsorption capacity, with maximum MB uptake observed at 45 °C. Elevated temperature increases molecular mobility, which enhances diffusion of MB toward available adsorption sites on BC and promotes stronger adsorbate–adsorbent interactions. The observed improvement in adsorption performance with temperature indicates an endothermic adsorption process, where increased thermal energy favors MB uptake.

3.5 Kinetic studies

Three kinetic models were employed to analyse the adsorption kinetics of MB, namely, the PFO, PSO, and Elovich kinetic models. The PFO model assumes a diffusion-controlled process occurring in the solid-liquid phase. PSO assumes the process is controlled by adsorption reaction at a liquid-solid interface. The PFO and PSO in linearized form is given by Eq. (3.3) and Eq. (3.4), which is as follows:

The PFO model, Eq. (3.3):

$$\ln (Q_e - Q_t) = lnQ_e - K_1 t$$

The PSO model, Eq. (3.4):

$$\frac{1}{Q_t} = \left(\frac{1}{kQ_e^2}\right)\frac{1}{t} + \frac{1}{Q_e}$$

The Elovich model was utilized to characterize adsorption under non-ideal conditions which assumes that the rate of solute adsorption decreases exponentially as the

amount of adsorbed solute increases. The equation for this model is expressed as follows in Eq. (3.5):

$$Q_t = \frac{\ln(\alpha\beta)}{\beta} + \frac{\ln(t)}{\beta}$$

where Q_e and Q_t are the dye amount adsorbed at equilibrium (mg/g), k represents the time, K_1 (min^{-1}) or K_2 (g/mg min) refers to the adsorption rate constant, α is the initial adsorption rate (mg/g), and β is the desorption coefficient (mg/g). To further investigate the diffusion mechanism, the intraparticle diffusion (IPD) model was applied, which can be expressed as follows in Eq. (3.6):

$$Q_t = K_p t^{0.5} + C$$

where K_p is the rate constant of the IPD kinetic model and C denotes the thickness of the boundary layer.

3.6 Isotherm studies

Equilibrium adsorption isotherms were used to calculate the maximum adsorption capacity (Q_m) using the Langmuir, Temkin, and Freundlich models. Each visualisation offers distinct insights based on various hypotheses on the isotherm's shape and the adsorbent surface. Monolayer adsorption on a homogeneous surface, with a constant adsorption energy across all sites, is the assumption of the Langmuir model. According to this paradigm, a site cannot experience any further adsorption after it has been full. Having K_L standing for the Langmuir binding constant (L/mol), which indicates the affinity between the adsorbent and the adsorbate, the linearised form of the Langmuir isotherm is shown in Eq. (3.7).

$$\frac{C_e}{Q_e} = \frac{C_e}{Q_m} + \frac{1}{K_L Q_m}$$

The strongest binding sites are occupied first, followed by sites with decreasing energy levels, according to the Freundlich equation, which describes how a solute adsorbs

from a solution onto a solid surface. This model depicts monolayer adsorption, which is distinguished by an uneven energy distribution across active sites. K_F, or the Freundlich constant, and n, or the heterogeneity factor, which represents the adsorption intensity, are both included in the Freundlich isotherm model. Eq. (3.8) provides a linear expression for the Freundlich isotherm model.

$$lnQ_e = \frac{\ln C_e}{n} - \ln K_F$$

The Temkin isotherm model is represented by Eq. (3.9). In this equation, T denotes the temperature, K_T and b are adjustable constants, and R is the universal gas constant.

$$Q_e = \frac{RT}{b} (\ln C_e + lnK_T)$$

where C_e is the equilibrium concentration of the dye solution (mg/L). K_T is the equilibrium binding constant (L/mol) associated with maximum binding energy, b relates to the heat of adsorption (J/mol), and R and T represent the universal gas constant (8.314 J/K·mol) and absolute temperature (K), respectively.

3.7 Cost analysis

A cost analysis was conducted to estimate the laboratory-scale production cost of food waste-derived BC. The assessment followed a bottom-up approach, in which all cost components were identified, quantified, and summed to obtain the total cost per kilogram of BC produced. Raw material cost was calculated based on the mass of mixed food waste required to produce 1 kg of BC after drying and carbonization. No purchase cost was assigned to the feedstock, as the food waste was collected as a discarded material. Water cost was included based on the total volume used during washing and sample preparation, calculated using the unit water tariff.

Energy cost was evaluated for drying and carbonization steps. Electrical energy consumption was estimated from oven and muffle furnace power ratings multiplied by operating time, with costs derived from the local electricity tariff. Energy used for grinding and sieving was estimated using equipment power ratings and processing duration. All energy inputs were normalized to cost per kilogram of final BC product. Labour cost was excluded, as all procedures were conducted in an academic laboratory setting without direct labour charges. Consumables, including crucibles, filter papers, glassware wear, and safety materials, were treated as fixed operational inputs and apportioned on a per-kilogram basis.

The total production cost of food waste-derived BC was calculated using the following expression:

Total cost (RM/kg) = Raw material cost + Water cost + Energy cost + Consumables cost

CHAPTER 4

RESULTS AND DISCUSSION

4.1 Characterization

4.1.1 FTIR

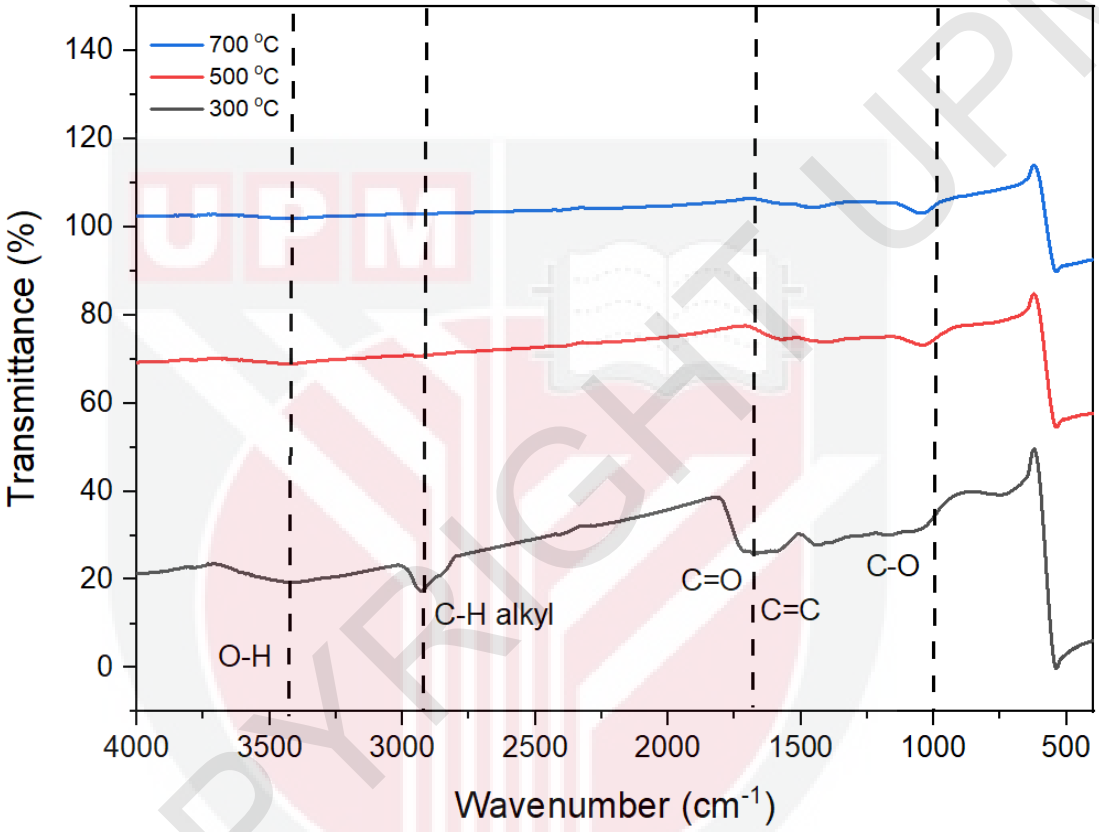

Fig. 4.1. FTIR spectra of food waste-derived BC prepared at carbonization temperatures of 300 °C, 500 °C, and 700 °C.

The FTIR spectra of BC prepared at 300 °C, 500 °C, and 700 °C as shown in Fig. 4.1 reveal systematic changes in surface chemistry with increasing carbonization temperature. A broad band around 3400 cm^{-1} corresponds to O-H stretching from hydroxyl groups and physically adsorbed water (Moeinfar et al., 2024). This band is most intense for BC300 and progressively weakens at higher temperatures, indicating thermal decomposition of surface hydroxyl groups. Absorption bands near 2920 cm^{-1} and 2850 cm^{-1} are assigned to aliphatic C-H stretching vibrations from alkyl groups.

The gradual attenuation of these bands with increasing temperature reflects the removal of volatile aliphatic components and the transition toward a more condensed carbon framework (Shao et al., 2023). The peak near 1700 cm^{-1}, associated with C=O stretching of carbonyl-containing functional groups, also decreases in intensity at higher carbonization temperatures, indicating a reduction in oxygen-containing surface functionalities. A distinct band around 1600 cm^{-1} corresponds to C=C stretching vibrations, characteristic of aromatic and conjugated structures. The increasing prominence of this band with temperature indicates enhanced aromatization and structural ordering of BC (D. Li et al., 2022). Aromatic domains in BC promote π–π interactions with the aromatic rings of MB, which contributes to improved adsorption performance, as reported previously (Vafakish et al., 2025). Additional band observed near 1000 cm^{-1} which attributed to C–O stretching vibrations originating from residual cellulose, hemicellulose, and lignin fragments (L.-Y. Chen et al., 2023). These features diminish with increasing carbonization temperature, confirming progressive decomposition of biomass-derived functional groups and their replacement by more stable aromatic carbon structures (Yang et al., 2023).

4.1.2 TGA

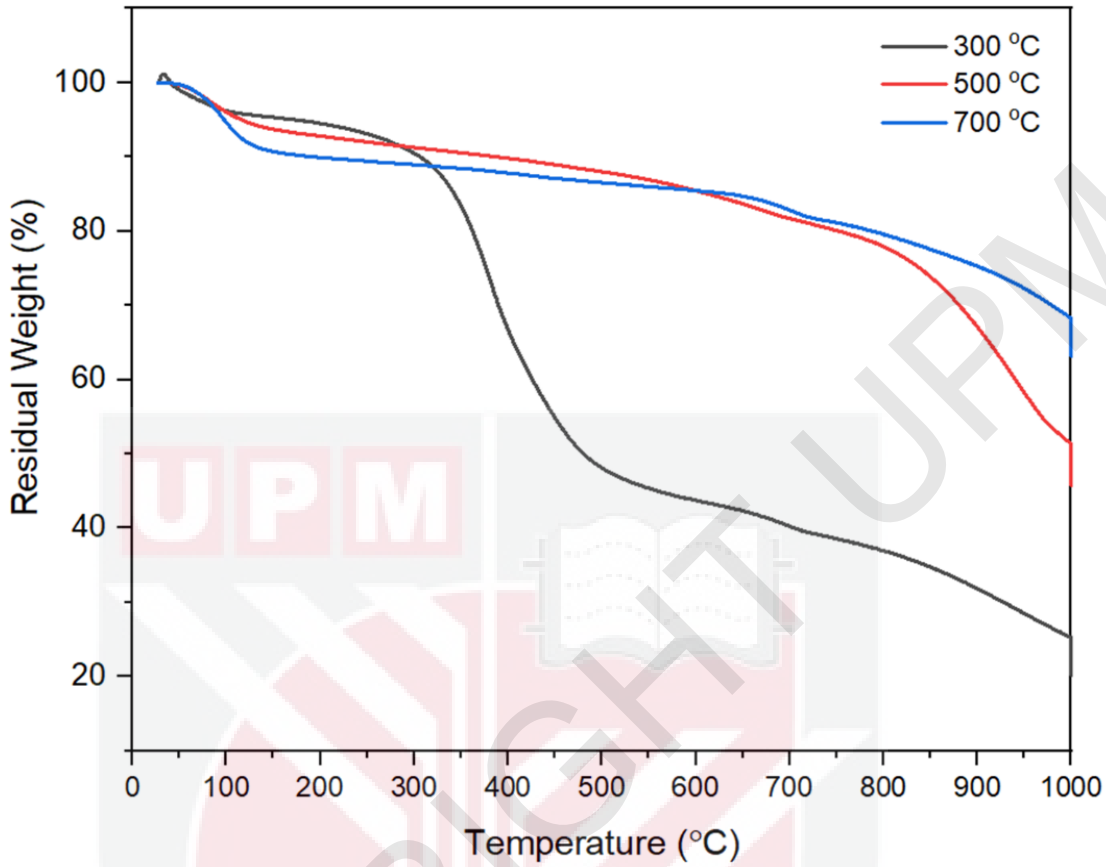

Fig. 4.2. TGA thermograms of food waste-derived BC prepared at different carbonization temperatures.

The thermal stability of food waste-derived BC carbonized at 300 °C, 500 °C, and 700 °C was evaluated using TGA, as illustrated in Fig. 4.2. All samples show a small mass loss below 150 °C, attributed to the removal of physically adsorbed moisture and light volatile compounds. This initial loss is typical for BC and reflects surface-bound species that do not contribute to the carbon framework (L.-Y. Chen et al., 2023). BC prepared at 300 °C exhibits pronounced mass loss between 350 °C and 500 °C. This region corresponds to the thermal decomposition of residual hemicellulose, cellulose, and other labile organic components that remain after low-temperature carbonization (Yang et al., 2023). The substantial weight reduction indicates incomplete

carbonization and a higher fraction of thermally unstable structures (L.-Y. Chen et al., 2023).

In contrast, BC produced at 500 °C and 700 °C shows markedly lower mass loss over the same temperature range, indicating more advanced carbonization and removal of unstable biomass constituents (L.-Y. Chen et al., 2023; Karce et al., 2025). These samples are dominated by condensed aromatic carbon structures, which display higher thermal resistance and decompose primarily above 600 °C. At 1000 °C, BC700 retains the highest residual mass, followed by BC500, confirming the formation of more thermally stable carbon matrices at higher carbonization temperatures.

The progressive improvement in thermal stability with increasing carbonization temperature reflects enhanced aromatization, increased fixed-carbon content, and reduced oxygen-containing functional groups. These structural changes result in a more rigid and stable carbon framework, consistent with previous reports on thermally treated BC systems (Vigdorowitsch et al., 2021; Yang et al., 2023).

4.1.3 FESEM

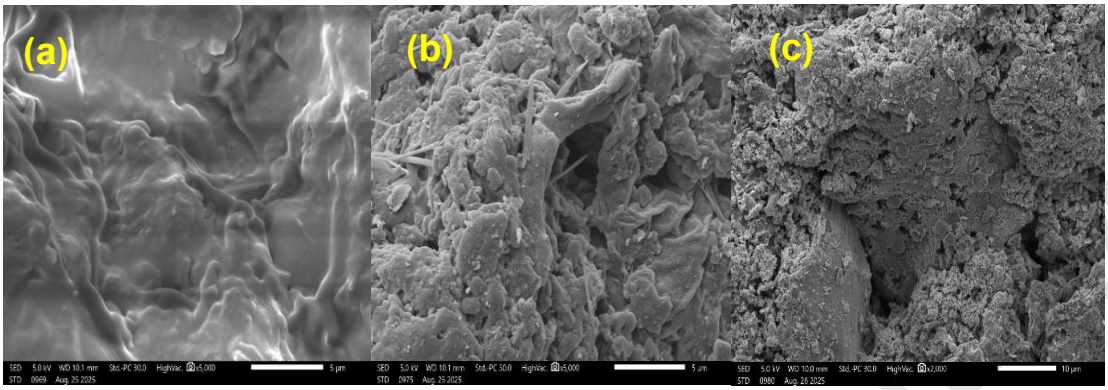

Fig. 4.3. FESEM micrographs of food waste-derived BC prepared at carbonization temperatures of (a) 300 °C, (b) 500 °C, and (c) 700 °C.

The surface morphology of BC prepared at 300 °C, 500 °C, and 700 °C was examined by FESEM, as shown in Fig. 4.3. At 300 °C as shown in Fig. 4.3 (a), BC shows a dense and compact surface with limited pore development. This morphology indicates incomplete carbonization at low temperature, where lignocellulosic components such as cellulose, hemicellulose, and lignin remain partially preserved (Lu et al., 2022; Nan et al., 2021). The restricted release of volatile matter results in a relatively smooth surface and poorly developed pore structure. Such features limit surface accessibility and reduce the number of effective adsorption sites, which is unfavorable for adsorption performance (Li et al., 2023).

At 500 °C as shown in Fig. 4.3 (b), BC exhibits a more heterogeneous and porous morphology. Visible cracks, flakes, and interconnected voids appear across the surface, reflecting extensive devolatilization and structural rearrangement during carbonization. This transformation is associated with the decomposition of cellulose and hemicellulose and the release of volatile gases, leaving behind a carbon-rich framework (K. Wang et al., 2023). The increased surface roughness and pore formation enhance surface area and create additional adsorption sites, which favor MB uptake (Fan et al., 2017).

At 700 °C as shown in Fig. 4.3 (c), BC displays a highly developed porous structure with pronounced surface roughness and fragmentation. Thin pore walls and expanded voids indicate extensive carbon restructuring and the collapse of thermally weak domains (Gao et al., 2020). This morphology reflects near-complete decomposition of organic matter and the formation of a stable carbon matrix. Enhanced pore interconnectivity and larger pore volume facilitate efficient diffusion and adsorption of MB molecules (Guo et al., 2024; H. Li et al., 2023). Higher carbonization temperature also promotes the removal of oxygen-containing functional groups, leading to increased structural stability and a more ordered carbon framework (Meng et al., 2024).

4.1.4 XRD

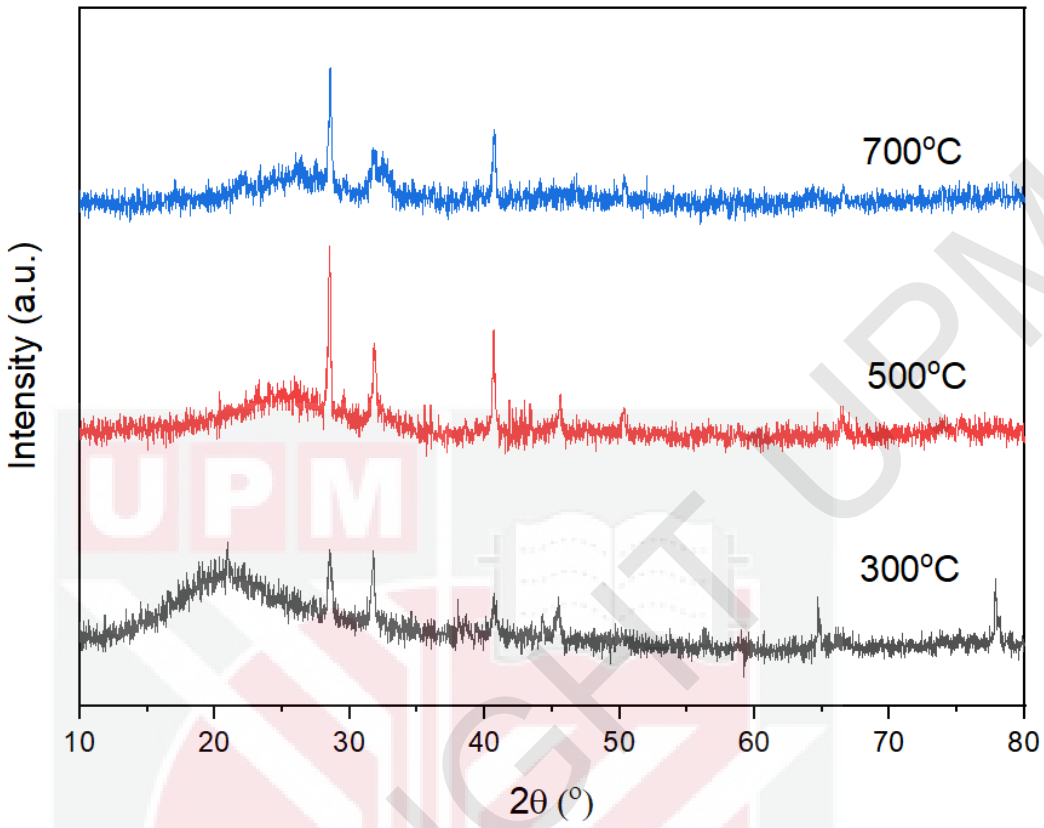

Fig. 4.4. XRD spectra of food waste-derived BC prepared at various carbonization temperatures.

The crystalline structure and phase transformation of the food waste-derived BC were characterized via XRD, as illustrated in Fig. 4.4. The diffractogram exhibits a characteristic profile of a heterogeneous, carbonaceous material containing both amorphous domains and well-defined inorganic crystalline phases. The broad hump between 21°- 28° corresponds to the (002) plane of disordered, graphitic carbon. The pronounced broadening of the (002) peak signifies a low degree of graphitic ordering and suggests that the carbonized framework consists of small, randomly oriented polyaromatic lamellae (Gao et al., 2020). This amorphous nature is characteristic of BCs produced at moderate temperatures, where the primary biomass components (cellulose and lignin) have undergone thermal degradation and aromatization without reaching the long-range ordering typical of synthetic graphite. The (002) peak in the

XRD pattern shows a systematic shift with increasing carbonization temperature, reflecting structural reorganization of the carbon matrix (Tripathi et al., 2022). This shift signifies a reduction in interlayer spacing, driven by progressive deoxygenation, condensation of aromatic domains, and partial graphitic ordering. The removal of volatile species and collapse of unstable functional groups allow carbon layers to pack more closely. At 300°C carbonization temperature, the (002) reflection appears at a lower 2θ value, indicating a larger interlayer spacing. This corresponds to a turbostratic carbon structure with high disorder, residual oxygenated groups, and incomplete aromatization (Sarwar et al., 2021). As the carbonization temperature increases, the (002) peak gradually shifts toward higher 2θ values.

Superimposed on the amorphous carbon humps are several sharp, high-intensity reflections that denote the presence of distinct crystalline mineral phases derived from the concentrated inorganic content of the food waste. Kitchen food waste is a complex feedstock, and its pyrolysis leads to BC with a diverse mineralogy. Common crystalline phases identified in BC, particularly from biomass and waste materials, often include quartz (SiO_2), calcite ($CaCO_3$), and other inorganic compounds originating from the ash content of the biomass (Beigmohammadi et al., 2024; D. Li et al., 2024). The occurrence of these minerals is of significant functional importance; they act as an *in-situ* inorganic template that prevents the total collapse of the carbon pores and may provide catalytic active sites.

4.2 Adsorption test

4.2.1 Comparison between adsorbents

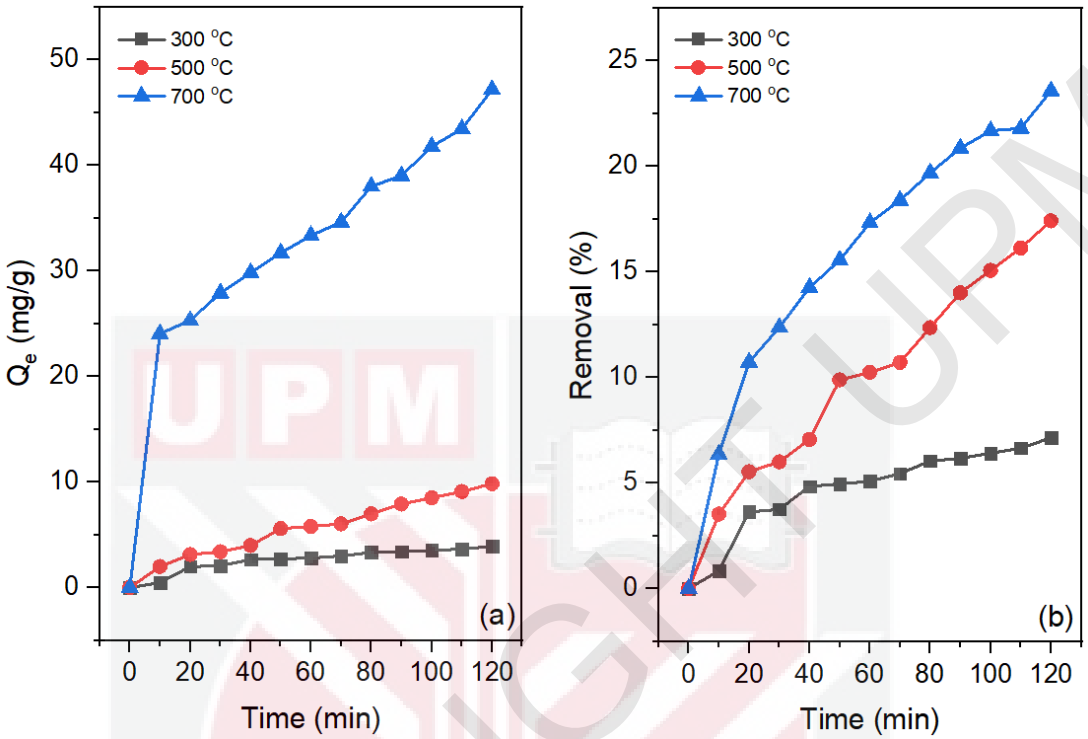

Fig. 4.5. Effect of carbonization temperature of food waste-derived BC on adsorption performance as a function of contact time, showing (a) adsorption capacity, Q_e (mg/g), and (b) MB removal efficiency (%). (Experimental conditions: $[MB]_0$ = 5 mg/L, adsorbent dosage = 10 mg, pH = 8.70, T = 25 °C.)

As shown in Fig. 4.5 (a), the adsorption performance differs significantly among the adsorbents prepared via carbonization at 300 °C, 500 °C, and 700 °C. For 700 °C carbonized adsorbents, rapid MB uptake occurs within the initial 10 - 20 min, followed by a slower approach to equilibrium, indicating an initial surface adsorption stage accompanied by subsequent diffusion into internal pores. The adsorbent carbonized at 300 °C exhibits the lowest adsorption capacity (Q_e) and removal efficiency throughout the contact period, suggesting limited pore development and fewer accessible active sites. In comparison, the adsorbent carbonized at 500 °C shows a moderate improvement in both Q_e and MB removal. The adsorbent carbonized at 700

°C demonstrates the highest adsorption capacity and removal efficiency, achieving the greatest Q_e values and removal percentages at 120 min. This enhanced performance is attributed to improved carbon structure, increased surface area, and greater pore accessibility resulting from higher carbonization temperature, which promotes more effective adsorbate - adsorbent interactions and faster mass transfer.

Furthermore, as illustrated in Fig. 4(b), the steeper initial increase in removal percentage for the 700 °C carbonized adsorbent confirms superior adsorption kinetics compared to the lower temperature counterparts. Although increasing carbonization temperature enhances adsorption performance, the rate of increase in Q_e becomes less pronounced at longer contact times as adsorption sites approach saturation and the concentration driving force decreases (Meng et al., 2024). This adsorption behavior is consistent with reported findings for MB removal using carbonized adsorbents, where higher carbonization temperatures yield improved adsorption efficiency due to enhanced pore formation and surface reactivity (Karce et al., 2025).

4.2.2 Influence of initial MB concentration

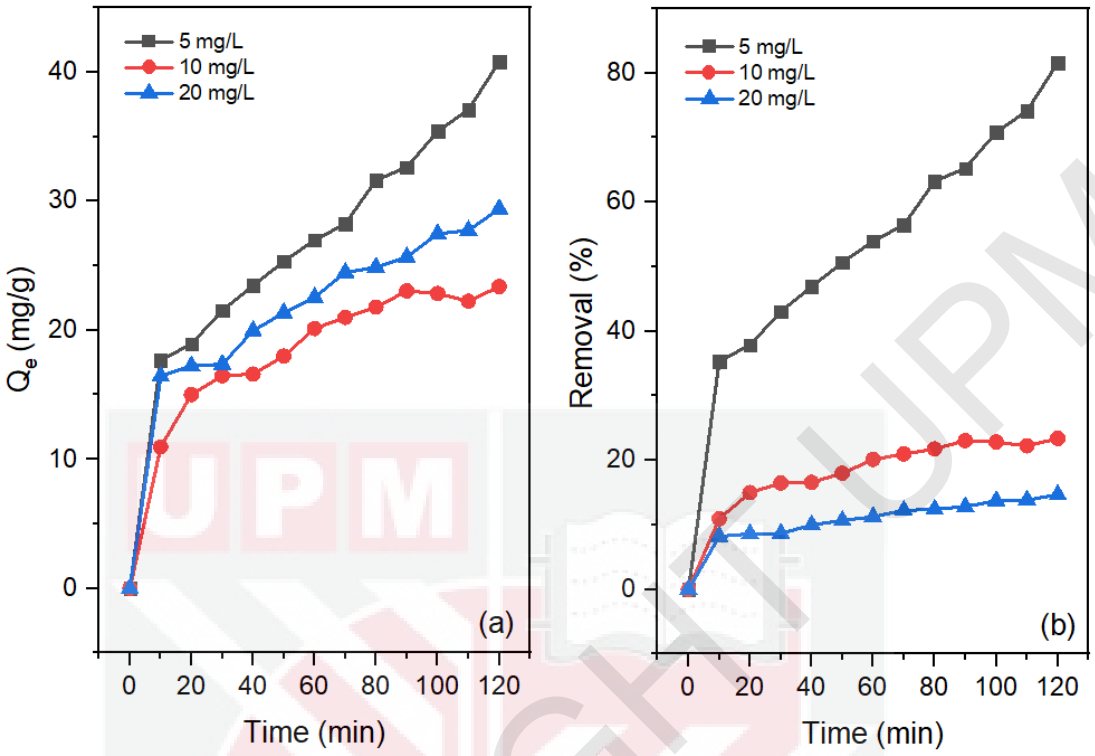

Fig. 4.6. Effect of initial MB concentration on adsorption performance of food waste-derived BC as a function of contact time, showing (a) adsorption capacity, Q_e (mg/g), and (b) MB removal efficiency (%), at initial MB concentrations of 5 mg/L, 10 mg/L, and 20 mg/L. (Experimental conditions: adsorbent dosage = 10 mg, pH = 8.70, T = 25 °C.)

As shown in Fig. 4.6(a) and (b), the adsorption performance of MB onto BC is strongly dependent on the initial dye concentration. Among the investigated concentrations, an initial MB concentration of 5 mg/L demonstrates the best overall adsorption performance. At this concentration, BC achieves the highest removal efficiency and a high adsorption capacity of approximately 40 mg/g within 120 min. This behavior is attributed to the high availability of active adsorption sites relative to the number of MB molecules in solution, which allows efficient dye-adsorbent interactions and minimizes competition for surface sites.

When the initial MB concentration is increased to 10 mg/L, the adsorption capacity increases gradually with contact time; however, the overall removal efficiency decreases compared to the 5 mg/L system. This trend indicates partial saturation of the adsorption sites, where the increased mass transfer driving force promotes MB uptake per unit mass of BC, but the number of dye molecules exceeds the available active sites. Consequently, a larger fraction of MB remains unadsorbed in solution, leading to a reduction in removal efficiency (Wu et al., 2023).

At an initial MB concentration of 20 mg/L, adsorption capacity continues to increase with time, but the removal percentage remains the lowest among the studied concentrations. This behavior reflects further saturation of adsorption sites and intensified competition among MB molecules for the limited active sites on the BC surface. In addition, diffusion limitations become more significant at higher dye concentrations, as MB molecules must diffuse deeper into the pore structure to access remaining adsorption sites, thereby restricting effective adsorption (Benamer-Oudih et al., 2023).

Overall, increasing the initial MB concentration enhances adsorption capacity due to the higher mass transfer driving force and increased frequency of dye-adsorbent interactions. However, excessive dye loading accelerates adsorption site saturation and increases competitive adsorption effects, resulting in reduced removal efficiency. The superior performance observed at 5 mg/L highlights that lower initial MB concentrations favor efficient utilization of available adsorption sites, leading to higher removal efficiency. These findings are consistent with previously reported studies, where increased dye concentration promoted adsorption capacity but reduced removal efficiency due to limited site availability and intensified competition among dye molecules (Ebrahimzadeh & Akbari, 2025; Lu et al., 2022).

4.2.3 Influence of adsorbent dosage

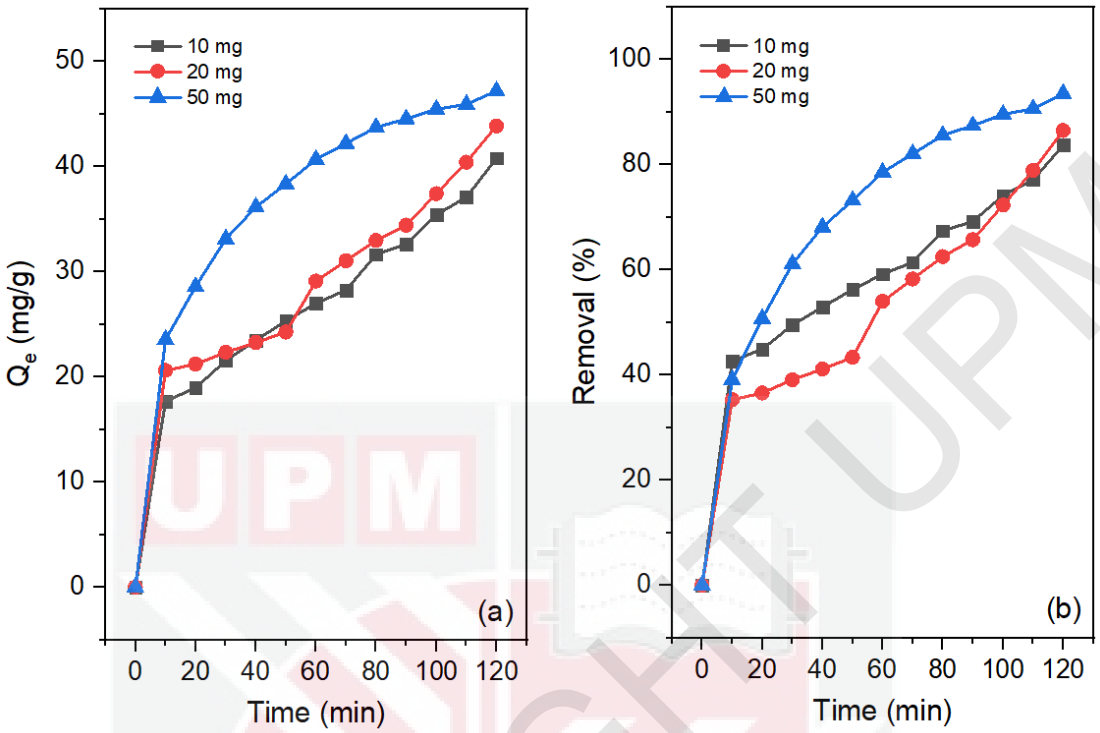

Fig. 4.7. Effect of BC dosage on MB adsorption as a function of contact time, showing (a) adsorption capacity, Q_e (mg/g), and (b) MB removal efficiency (%), at BC dosages of 10 mg, 20 mg, and 50 mg. (Experimental conditions: $[MB]_0$ = 5 mg/L, pH = 8.70, T = 25 °C.)

As shown in Fig. 4.7(a) and (b), BC dosage exerts a significant influence on both adsorption capacity (Q_e) and MB removal efficiency. For all studied dosages, rapid MB uptake is observed within the first 10–20 min, followed by a more gradual increase toward equilibrium. This behavior indicates that adsorption initially occurs through fast occupation of readily available surface sites, after which the rate becomes controlled by diffusion of MB molecules into the internal pore structure of BC.

At a BC dosage of 10 mg, Q_e increases steadily with contact time, reaching approximately 40 mg/g after 120 min, accompanied by a removal efficiency of about 85%. The relatively lower dosage limits the number of available adsorption sites, which

constrains MB uptake and results in slower adsorption kinetics and reduced overall removal efficiency compared to higher dosages.

When the BC dosage is increased to 20 mg, both adsorption capacity and removal efficiency are enhanced. The final Q_e reaches approximately 44 mg/g, while the removal efficiency approaches 88% at 120 min. This improvement can be attributed to the increased number of accessible adsorption sites and expanded effective surface area, which facilitate greater interaction between MB molecules and the adsorbent (Z. Shao et al., 2025).

The highest BC dosage of 50 mg exhibits the most pronounced adsorption performance, achieving a Q_e of approximately 47 mg/g and exceeding 90% MB removal within 120 min. As shown in Fig. 4.7(b), the removal percentage at 50 mg increases rapidly, surpassing 60% within the first 40 min. This rapid uptake confirms enhanced mass transfer and improved site availability at higher adsorbent loading, which accelerates MB diffusion and adsorption.

Although increasing BC dosage leads to higher overall MB removal, the incremental increase in Q_e from 20 mg to 50 mg becomes less significant at longer contact times. This trend suggests partial overlap of adsorption sites and a reduction in the effective driving force for adsorption when the number of available sites exceeds the number of MB molecules in solution. Such behavior is commonly observed in adsorption systems and is consistent with previous reports on similar BC-based adsorbents (Muteeb et al., 2025).

4.2.4 Influence of pH of solution

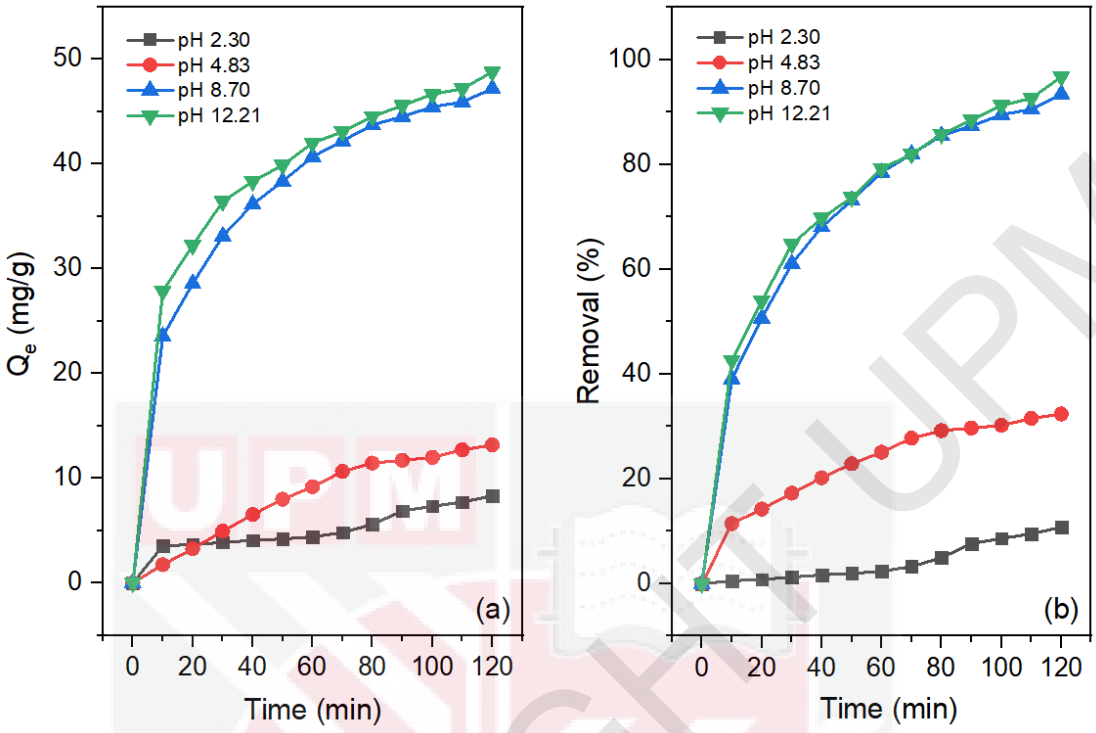

Fig. 4.8. Effect of solution pH on MB adsorption by food waste-derived BC as a function of contact time, showing (a) adsorption capacity, Q_e (mg/g), and (b) MB removal efficiency (%), at pH 2.30, 4.83, 8.70, and 12.21. (Experimental conditions: $[MB]_0$ = 5 mg/L, adsorbent dosage = 50 mg, T = 25 °C.)

As shown in Fig. 4.8(a), the adsorption capacity (Q_e) of MB onto BC exhibits a strong dependence on the solution pH. Under acidic conditions (pH 2.30 and 4.83), Q_e remains relatively low throughout the contact time and increases only gradually. At pH 2.30, adsorption is severely limited, with Q_e remaining below 10 mg/g after 120 min, while a slightly higher but still modest uptake is observed at pH 4.83, where Q_e remains below 15 mg/g. These results indicate that acidic conditions are unfavorable for MB adsorption onto BC.

In contrast, a pronounced enhancement in adsorption performance is observed at alkaline pH values of 8.70 and 12.21. Rapid MB uptake occurs during the initial adsorption stage, followed by a gradual approach to equilibrium, resulting in

substantially higher adsorption capacities. After 120 min, Q_e at pH 8.70 and 12.21 reaches approximately 47- 49 mg/g, indicating effective utilization of the available adsorption sites. The rapid initial uptake suggests strong affinity between MB molecules and the BC surface under alkaline conditions.

A similar pH-dependent trend is observed in the removal efficiency profiles shown in Fig. 4.8(b). Removal percentages are minimal at pH 2.30, increase moderately at pH 4.83, and rise sharply at higher pH values. At pH 8.70 and 12.21, removal efficiencies exceed 90 % within 120 min, confirming the superior adsorption performance under alkaline conditions.

The enhanced adsorption observed at higher pH values can be attributed to the deprotonation of surface functional groups on BC, which generates negatively charged sites that promote strong electrostatic attraction with the cationic MB molecules. In contrast, at low pH, extensive protonation of the BC surface reduces the availability of negatively charged sites and leads to electrostatic repulsion, as well as competition between excess protons and MB molecules for active adsorption sites. These combined effects significantly suppress MB adsorption under acidic conditions. Similar pH-dependent adsorption behavior has been reported in previous studies, highlighting the critical role of surface charge and electrostatic interactions in MB adsorption systems (Vojnović et al., 2022).

4.2.5 Influence of temperature of solution

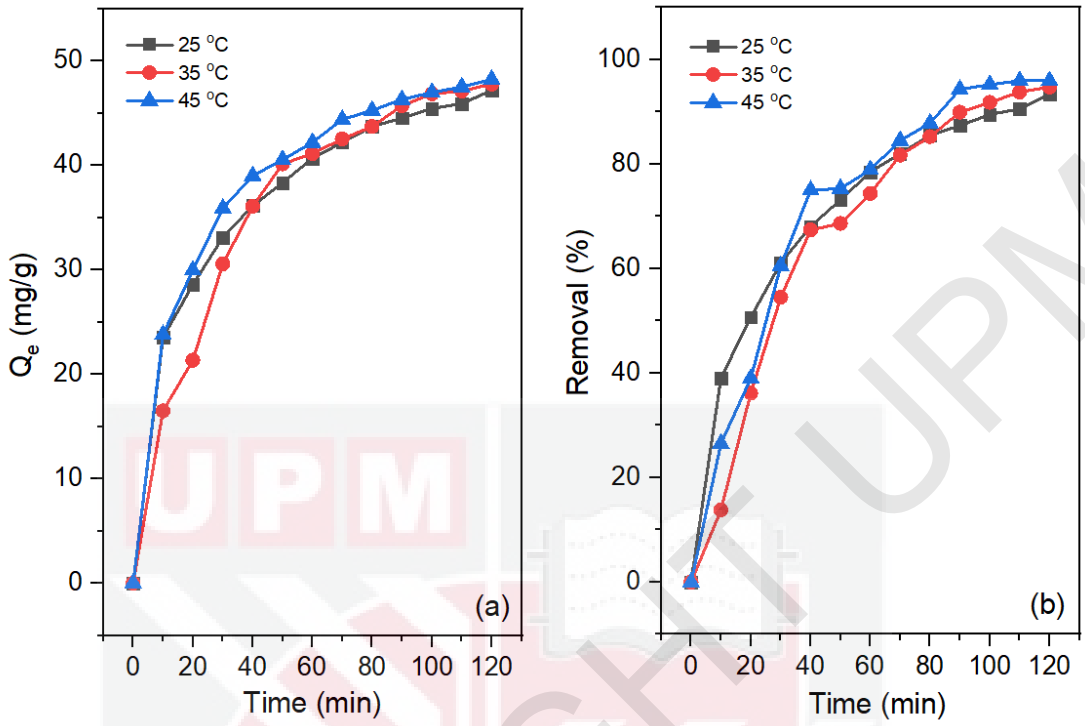

Fig. 4.9. Effect of solution temperature on MB adsorption by food waste-derived BC as a function of contact time, showing (a) adsorption capacity, Q_e (mg/g), and (b) MB removal efficiency (%), at 25 °C, 35 °C, and 45 °C. (Experimental conditions: $[MB]_0$ = 5 mg/L, adsorbent dosage = 50 mg, pH = 12.21.)

As shown in Fig. 4.9(a), Q_e exhibits a clear dependence on solution temperature, indicating that the adsorption of methylene blue (MB) onto BC is thermally influenced. At 25 °C, the adsorption process proceeds relatively slowly, particularly during the initial stage, where the uptake rate is limited by lower molecular motion and slower diffusion of MB molecules from the bulk solution to the adsorbent surface. The system gradually approaches equilibrium, reaching a final Q_e of approximately 45 mg/g after 120 min. This lower equilibrium capacity suggests that, at reduced temperatures, fewer active sites are effectively utilized and the driving force for mass transfer is weaker.

When the temperature is increased to 35 °C, both the adsorption rate and equilibrium capacity improve noticeably. The steeper rise in Q_e during the early contact time

reflects faster external mass transfer and enhanced intraparticle diffusion, allowing MB molecules to access internal pores more efficiently. Consequently, the equilibrium Q_e increases to about 47 mg/g. This behavior indicates that moderate heating provides sufficient thermal energy to overcome diffusion barriers and promotes stronger interactions between MB molecules and functional groups on the BC surface.

At the highest temperature of 45 °C, the adsorption process becomes most efficient, with the fastest uptake rate and the highest equilibrium Q_e, approaching 48–49 mg/g. Equilibrium is reached earlier compared to lower temperatures, suggesting that adsorption sites are rapidly occupied under these conditions. The observed enhancement can be attributed to increased molecular mobility of MB, reduced solution viscosity, and improved pore diffusion, which collectively facilitate the transport of MB molecules into the internal structure of BC. These results imply that the adsorption process is endothermic in nature and benefits from elevated temperatures, consistent with previously reported studies (Kuang et al., 2020; J. Wang et al., 2023).

A similar temperature-dependent trend is evident in the removal efficiency profiles shown in Fig. 4.9(b). At 25 °C, MB removal increases steadily with time but reaches only about 90% after 120 min, indicating incomplete utilization of adsorption sites within the studied contact time. The slower initial increase suggests that mass transfer resistance plays a more dominant role at lower temperatures, limiting the overall removal efficiency.

In contrast, increasing the temperature to 35 °C significantly enhances the removal performance. The removal efficiency rises more rapidly during the early stages and exceeds 95% at equilibrium. At 45 °C, the system exhibits the steepest initial increase in removal efficiency, achieving high MB removal within a much shorter contact time. The earlier plateau observed at higher temperatures indicates that adsorption equilibrium is attained more quickly, reflecting improved adsorption kinetics and more effective occupation of available active sites.

The comparatively lower removal efficiency at 25 °C can be attributed to slower diffusion rates, reduced collision frequency between MB molecules and the BC surface, and weaker adsorbate–adsorbent interactions due to insufficient thermal energy. Overall, the results from both Q_e and removal efficiency analyses confirm that higher temperatures favor MB adsorption onto BC by enhancing kinetic processes and mass transfer, in agreement with literature findings (Kuang et al., 2020).

4.3 Adsorption kinetic

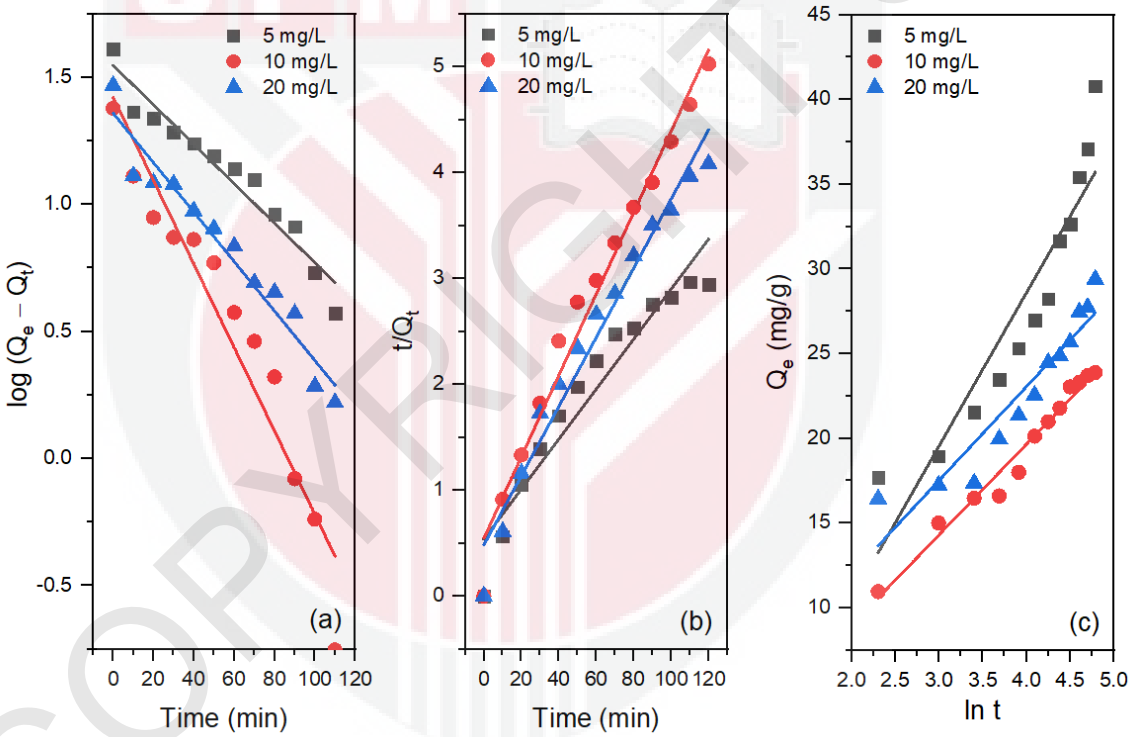

Fig. 4.10. Kinetic analysis of MB adsorption onto food waste-derived BC. (a) PFO kinetic plots, log (Q_e − Q_t) versus time, at initial MB concentrations of 5 mg/L, 10 mg/L, and 20 mg/L. (b) PSO kinetic plots, t/Q_t versus time, at corresponding initial MB concentrations. (c) Elovich kinetic plots, Q_e versus ln t.

The adsorption kinetics of MB onto BC were evaluated at initial concentrations of 5 mg/L, 10 mg/L, and 20 mg/L using the PFO, PSO, and Elovich models with the

corresponding kinetic parameters summarized in Table 4.1. The combined graphical and quantitative analyses provide clear insight into the governing adsorption mechanism. As shown in Fig. 4.10(a), the PFO plots display noticeable deviations from linearity at all concentrations, particularly at longer contact times. This observation is supported by Table 4.1, where although moderate correlation coefficients are obtained (R^2 = 0.9149–0.9432), the calculated equilibrium adsorption capacities are severely underestimated. The $Q_{e,cal}$ values derived from the PFO model range only from 3.89 to 4.70 mg/g, which are far lower than the experimentally observed capacities. In addition, the negative K_1 values lack physical significance. These discrepancies confirm that the PFO model fails to represent the adsorption process accurately and that MB uptake is not governed solely by physical adsorption or diffusion-controlled mechanisms (Ho and McKay, 1999; Wang et al., 2023c).

In contrast, Fig. 4.10(b) shows excellent linearity for the PSO plots across all concentrations, indicating strong model applicability. This conclusion is reinforced by the kinetic parameters in Table 4.1, where high correlation coefficients are obtained, particularly at 10 mg/L (R^2 = 0.9762) and 20 mg/L (R^2 = 0.9650). Importantly, the PSO-calculated equilibrium capacities ($Q_{e,cal}$ = 26.01–42.35 mg/g) are in close agreement with experimental values, confirming the robustness of the PSO model. The PSO rate constants increase with increasing MB concentration, reflecting enhanced collision frequency but also increased competition for active sites. These results indicate that chemisorption governs the rate-limiting step, involving valence interactions between MB molecules and surface functional groups on BC (Ho & McKay, 1999).

Further insight into surface heterogeneity is provided by the Elovich model in Fig. 4.10(c). The Elovich plots exhibit good linearity at 5 mg/L and 10 mg/L, with high correlation coefficients (R^2 = 0.9523 and 0.9715, respectively), while a reduced fit is observed at 20 mg/L (R^2 = 0.8797). The high Elovich α values, particularly at 5 mg/L (58,333.4 mg/g·min), indicate rapid initial adsorption on highly energetic surface sites.

The progressive decrease in α and the increase in β with rising MB concentration reflect gradual site occupation and a faster decline in adsorption rate as surface coverage increases. This behavior confirms adsorption on an energetically heterogeneous BC surface, where high-energy sites are occupied first, followed by adsorption on less active sites as loading increases.

Overall, the kinetic analyses indicate that the adsorption behavior of MB onto BC depends on the initial dye concentration. At lower MB concentrations, the good agreement with the Elovich model highlights the importance of surface heterogeneity and rapid adsorption on high-energy active sites. As the concentration increases, the PSO model provides a superior fit, demonstrating that chemisorption becomes the dominant rate-controlling mechanism due to increased interaction between MB molecules and functional groups on the BC surface. This concentration-dependent behavior confirms that MB adsorption onto BC is governed by chemisorption on a heterogeneous surface. These findings are consistent with the diverse surface functional groups identified by FTIR and the non-uniform pore structure observed in FESEM analysis.

Table 4.1. Kinetic parameters for MB adsorption onto food waste-derived BC derived from PFO, PSO, and Elovich models at different initial MB concentrations.

Kinetic model	**Parameters**	**[MB]**		
		5 mg/L	**10 mg/L**	**20 mg/L**
PFO	K_1	-0.00019425	-0.00041025	-0.00024325
	$Q_{e'cal}$ (mg/g)	4.698954325	4.141798029	3.890392297
	R^2	0.93487	0.91489	0.94321

PSO	K_2	0.001035272	0.002698406	0.002212497
	$Q_{e'cal}$ (mg/g)	42.35493435	26.00780234	30.59039462
	R^2	0.91426	0.97618	0.96503
Elovich	α	58333.4	13765.3	1852.98
	β	0.110572011	0.1587	0.180761875
	R^2	0.95226	0.97148	0.8797

4.4 Adsorption Isotherm

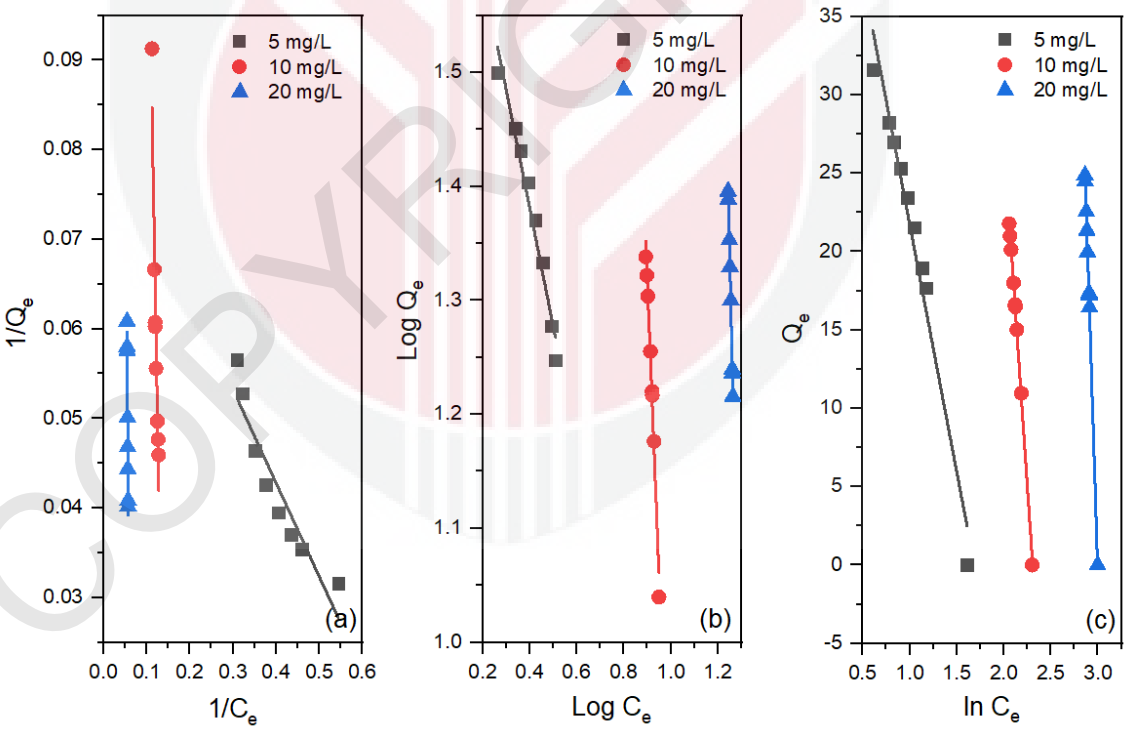

Fig. 4.11. Adsorption isotherm analysis for MB adsorption onto food waste-derived BC at initial MB concentrations of 5 mg/L, 10 mg/L, and 20 mg/L, showing (a) Langmuir plots ($1/Q_e$ versus $1/C_e$), (b) Freundlich plots (log Q_e versus log C_e), and (c) Temkin plots (Q_e versus ln C_e).

The equilibrium adsorption behavior of MB onto BC was analyzed using Langmuir, Freundlich, and Temkin isotherm models, with the model parameters summarized in Table 4.2. As shown in Fig. 4.11(a), the Langmuir plots display only moderate linearity across all concentrations, with correlation coefficients ranging from 0.8681 to 0.9843. Deviations from ideal linearity become more pronounced at higher equilibrium concentrations, indicating that the adsorption system does not strictly satisfy Langmuir assumptions of monolayer adsorption on a homogeneous surface with identical adsorption sites. Although the Langmuir model provides estimates of monolayer capacity, the variation in Q_{max} values (2.06 –11.83 mg/g) and the non-ideal fitting suggest the presence of surface heterogeneity and possible multilayer adsorption effects, consistent with observations reported for BC-based adsorbents (Foo & Hameed, 2010).

The Freundlich model exhibits improved fitting relative to the Langmuir model, as shown in Fig. 4.11(b). High correlation coefficients are obtained across all concentrations, with R^2 values ranging from 0.9655 to 0.9960, indicating adsorption on a heterogeneous surface with non-uniform energy distribution. The Freundlich constants K_F show large variability with concentration, suggesting changes in adsorption affinity as surface coverage increases. Additionally, the negative n values indicate unfavorable or complex adsorption behavior, further supporting deviation from ideal monolayer adsorption and highlighting the heterogeneous nature of the BC surface. These findings are consistent with the presence of multiple adsorption sites associated with diverse surface functional groups on BC, in agreement with FTIR and FESEM observations (Vigdorowitsch et al., 2021).

Among the three models, the Temkin isotherm provides the best overall description of the equilibrium data, as shown in Fig. 4.11(c). The Temkin plots display strong linearity across all concentrations, with high correlation coefficients, particularly at 5 mg/L (R^2 = 0.9967) and 20 mg/L (R^2 = 0.9995). The Temkin constants indicate that adsorption heat

decreases linearly with increasing surface coverage, reflecting significant adsorbate–adsorbent interactions during MB uptake. This behavior suggests that adsorption is governed by interaction energy effects rather than ideal monolayer coverage, implying contributions from electrostatic attraction, π–π interactions between aromatic structures of BC and MB, and surface complexation mechanisms. Similar Temkin-dominated adsorption behavior has been reported for interaction-controlled dye adsorption systems (Mozaffari Majd et al., 2022).

Overall, the isotherm analysis confirms that MB adsorption onto food waste-derived BC occurs on a heterogeneous surface and is strongly influenced by adsorbate–adsorbent interactions. While the Langmuir model provides a simplified capacity estimate, the Freundlich and Temkin models better capture the non-ideal, interaction-driven nature of the adsorption process, with the Temkin model offering the most accurate representation of equilibrium behavior.

Table 4.2. Isotherm parameters for MB adsorption onto food waste-derived BC obtained from Langmuir, Freundlich, and Temkin models at different initial MB concentrations.

Model	**Parameters**	**[MB]**		
		5 mg/L	**10 mg/L**	**20 mg/L**
Langmuir	Q_{max}	11.82592242	2.544917799	2.062536094
	K_L	-0.809729005	-0.143143369	-0.062123923
	R^2	0.86812	0.91645	0.98431
Freundlich	K_F	62.58208095	927363.5031	2.12119E+12
	n	-0.963771817	-1.93556E-06	-0.113794642

	R^2	0.96554	0.97858	0.99599
Temkin	A	0.031	0.0471	0.0596
	B	-31.60058	-88.5546	-187.43056
	R^2	0.996737	0.9983	0.9995

4.5 Regeneration Test

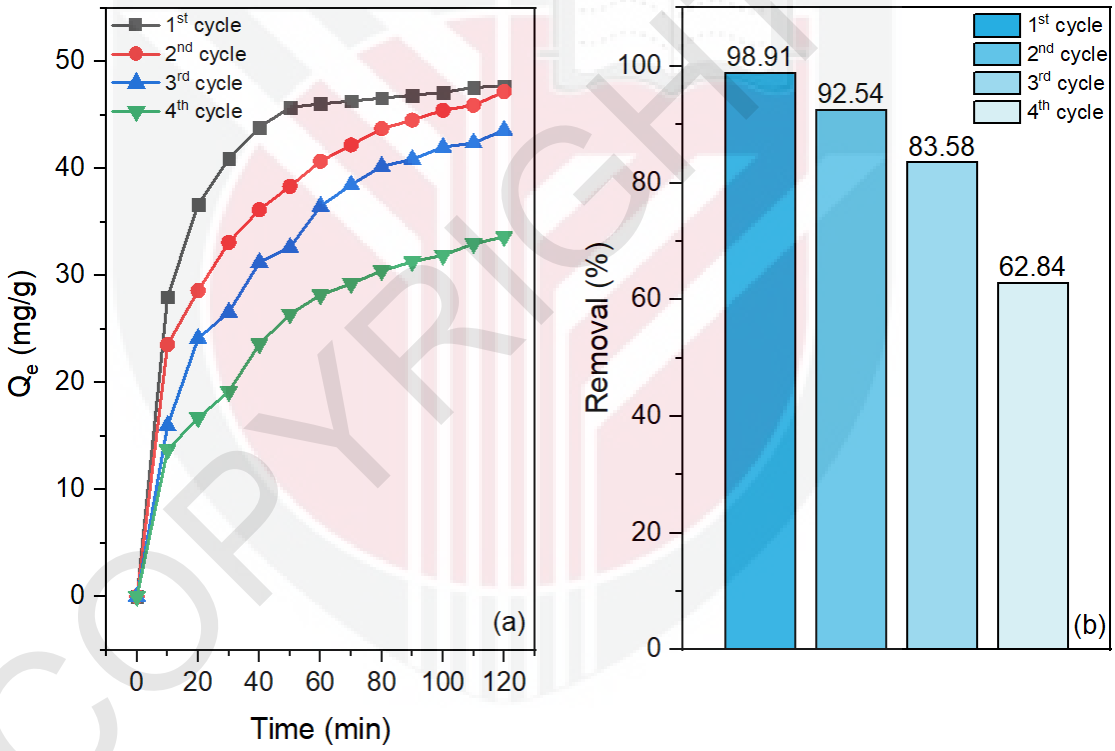

Fig. 4.12. Regeneration performance of food waste-derived BC during repeated MB adsorption–desorption cycles, showing (a) adsorption capacity, Q_e (mg/g), as a function of contact time and (b) MB removal efficiency (%) over four consecutive cycles.

The regeneration performance of BC was evaluated over four consecutive adsorption–desorption cycles, and the results are presented in Fig. 4.12(a) and Fig. 4.12(b). As shown in Fig. 4.12(a), a clear and progressive decline in adsorption capacity is observed with repeated reuse of BC, indicating gradual deterioration of adsorption efficiency. During the first cycle, BC exhibits rapid MB uptake, with a steep increase in Q_e during the initial contact period, reflecting abundant available active sites and strong affinity between MB molecules and the BC surface. Equilibrium is reached within 120 min, with the highest Q_e of approximately 48-49 mg/g, demonstrating the excellent initial adsorption performance of the freshly prepared BC.

In the second cycle, although the overall adsorption trend remains similar, the equilibrium adsorption capacity decreases slightly to around 45 mg/g. The uptake rate remains relatively fast in the early stage but slows down earlier compared to the first cycle, suggesting partial loss or blockage of adsorption sites following regeneration. In the third cycle, a more noticeable reduction is observed, with equilibrium Q_e declining further to approximately 42–43 mg/g. This indicates cumulative effects of repeated adsorption–desorption processes, including incomplete desorption of MB molecules and gradual reduction in the number of accessible active sites.

A pronounced decline in adsorption capacity is evident in the fourth cycle, where Q_e drops significantly to approximately 33–35 mg/g. The adsorption curve becomes less steep throughout the entire contact time, indicating slower adsorption kinetics and reduced surface activity. This substantial decrease is attributed to irreversible binding of MB molecules, pore blockage by residual dye, and possible structural or chemical alteration of surface functional groups during repeated regeneration steps. Such changes reduce pore accessibility and weaken adsorbate–adsorbent interactions, ultimately limiting adsorption performance in later cycles.

A consistent deterioration trend is observed in the removal efficiency data presented in Fig. 4.12(b). The first cycle exhibits the highest MB removal efficiency of 98.91%,

confirming the strong adsorption capability of fresh BC. In the second cycle, removal efficiency decreases moderately to 92.54%, indicating that most adsorption sites remain active despite some loss in performance. However, a more substantial decline occurs in the third cycle, where removal efficiency drops to 83.58%, reflecting reduced availability of effective adsorption sites and increased mass transfer resistance. In the fourth cycle, removal efficiency decreases sharply to 62.84%, highlighting significant degradation of adsorption effectiveness after multiple reuse cycles.

The sharp reduction observed after the third cycle suggests that repeated regeneration leads to diminishing surface accessibility and exhaustion of high-energy adsorption sites. This behavior is commonly reported for BC and activated carbon adsorbents and is primarily associated with irreversible dye binding, pore fouling, and gradual degradation or chemical modification of surface functional groups responsible for adsorption (Louros et al., 2022). Additionally, repeated exposure to regeneration conditions may weaken the adsorbent structure, further contributing to performance loss.

Despite the observed decline, BC retains more than 90% removal efficiency after one regeneration cycle and more than 80% after two cycles, demonstrating reasonable reusability and operational stability. These results highlight the practical potential of food waste-derived BC as a reusable adsorbent for MB removal in wastewater treatment applications. However, the gradual performance deterioration also indicates the need for improved regeneration strategies, such as optimized desorption agents or milder regeneration conditions, to restore adsorption capacity and extend the service life of BC over prolonged reuse.

4.6 FTIR Spectrum of Regenerated BC700

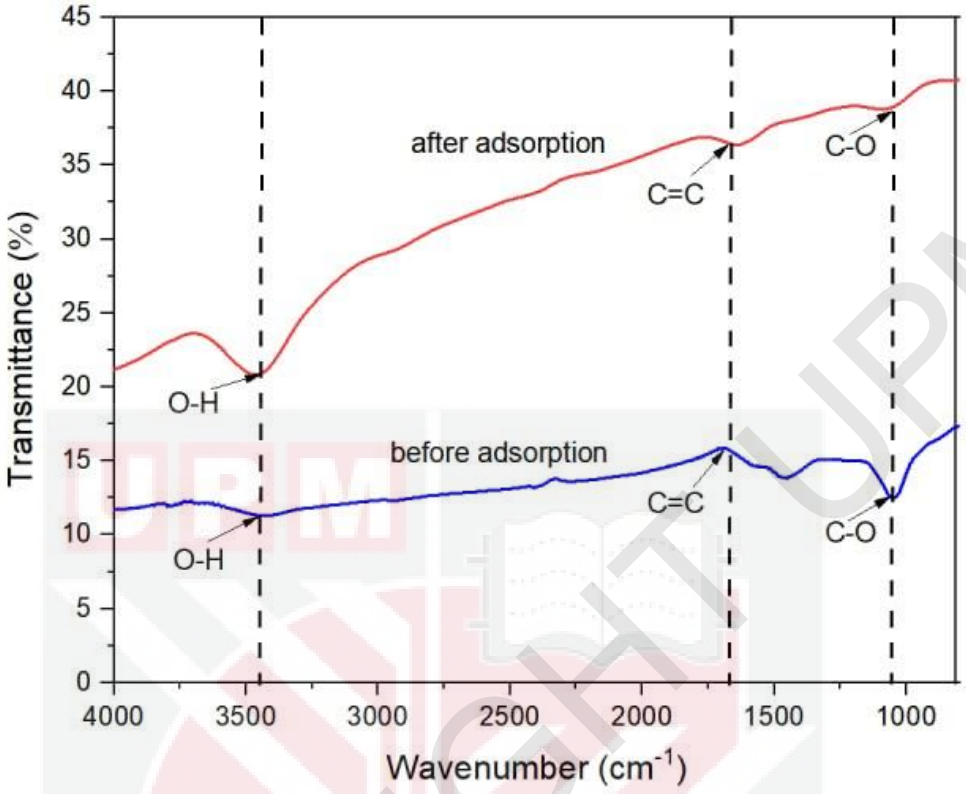

Fig. 4.13. FTIR spectra of food waste-derived BC prepared at 700 °C before and after adsorption.

The FTIR spectra of regenerated BC700 before and after adsorption are presented in Fig. 4.13, revealing notable changes in surface functional groups that reflect the adsorption mechanism and the effect of regeneration. As shown in the spectra, several characteristic peaks associated with oxygen-containing and aromatic functional groups are observed, indicating that the surface chemistry of BC700 plays an important role in the adsorption process.

Before adsorption, a broad absorption band is observed around 3400–3500 cm^{-1}, corresponding to the stretching vibration of O–H groups from hydroxyl and adsorbed water molecules. After adsorption, this band shows a slight shift and change in intensity, suggesting the involvement of hydroxyl groups in interactions with MB

molecules. This variation indicates that hydrogen bonding or electrostatic interactions may contribute to the adsorption process.

In the region around 1500-1600 cm^{-1}, the presence of the C=C stretching vibration associated with aromatic structures is evident in both spectra. After adsorption, the intensity of this peak becomes more pronounced, implying enhanced π–π interactions between the aromatic rings of MB and the graphitic domains of BC700. This observation confirms that the aromatic carbon framework of BC700 plays a significant role in stabilizing adsorbed MB molecules through π–π stacking interactions.

Furthermore, the absorption band near 1000-1100 cm^{-1}, attributed to C-O stretching vibrations of alcohol, ether, or phenolic groups, also exhibits noticeable changes after adsorption. The slight shift and alteration in peak intensity indicate that these oxygen-containing functional groups participate in the adsorption process, possibly through complexation or surface interactions with MB molecules.

Overall, the comparison between the spectra before and after adsorption demonstrates that although BC700 undergoes regeneration, its key functional groups remain active and capable of interacting with MB molecules. The observed peak shifts and intensity changes confirm that adsorption on regenerated BC700 is governed by a combination of hydrogen bonding, π–π interactions, and surface functional group involvement. These results indicate that regeneration does not significantly destroy the surface chemistry of BC700, but repeated adsorption–desorption cycles may gradually modify functional groups, which could contribute to the slight reduction in adsorption performance observed in regeneration studies.

4.7 Comparison with other adsorbents

Table 4.3 benchmarks the food waste-derived BC developed in this study against representative BC-based adsorbents reported for MB removal. The comparison highlights adsorption capacity, operating conditions, kinetic and isotherm behavior, and regeneration performance, allowing assessment of competitiveness under practical constraints.

The food waste-derived BC achieves an equilibrium adsorption capacity of 47–49 mg/g with removal exceeding 95% at low initial MB concentrations of 5–20 mg/L and a contact time of 120 min. This performance is comparable to several reported BC systems that operate at substantially higher initial concentrations, longer contact times, or under engineered conditions. Notably, the present BC attains this level of performance without chemical activation, surface doping, or post-treatment, relying solely on thermal carbonization of mixed food waste.

Several literature systems report higher Q_{max} values, including PTGA BC, BDSS, AC, and KOH-activated rice straw carbon. These materials achieve elevated capacities through intensive processing routes such as hydrothermal treatment, alkali activation, or high-temperature activation up to 800 °C. Such approaches increase surface area and porosity but also raise energy demand, chemical consumption, and production cost. In contrast, the present BC shows competitive MB uptake under milder synthesis conditions, which strengthens its relevance for scalable and low-cost applications.

Kinetic behavior further supports this positioning. MB adsorption on the food waste-derived BC follows PSO and Elovich models, indicating chemisorption on a heterogeneous surface. This behavior aligns with many high-performing BC systems while distinguishing the present material from adsorbents governed primarily by intraparticle diffusion or physisorption. The Temkin-dominated isotherm response observed for this BC indicates interaction-controlled adsorption, consistent with the

presence of diverse surface functional groups derived from mixed food waste. Many comparative studies rely on Langmuir fitting alone, which assumes surface homogeneity and ideal monolayer coverage, conditions not fully representative of real BC systems.

Regeneration performance also supports competitiveness under practical use. The food waste-derived BC retains more than 90% removal efficiency after the first cycle and over 80% after two cycles, with predictable decline by the fourth cycle. This stability compares favorably with chemically activated or engineered carbons that often exhibit sharper performance loss after limited reuse. The absence of harsh regeneration steps further supports operational simplicity.

Table 4.3. Comparative performance of food waste-derived BC and selected BC-based adsorbents for MB removal.

Adsorbent	Feedstock	Preparation / Modification	[MB]	Contact time	Q_{max} / Q_e (mg/g)	Removal (%)	Kinetic model	Isotherm model	Regeneration	Reference
Food waste-derived BC	Mixed food waste	Carbonization at 300–700 °C	5–20	120 min	47–49 (Q_e)	>95	PSO, Elovich	Temkin	4 cycles (62.8% at 4th)	**This study**
Kitchen-waste BC	Orange peel, potato peel, banana peel, coffee residue (25% each)	Carbonization 400 °C, 1 h	10–180	0.5–24 h	~44.8 (Q_e)	99.2–99.8	NR	Langmuir	NR	(Kataya et al., 2025)

FEBC	Manila tamarind seed coat	Pyrolysis 550 °C	50	480 min	106.85 (Q_{max})	94	IPD-controlled	Langmuir	NR	(Chutani et al., 2026)
FEBC	Manila tamarind seed coat	Pyrolysis 550 °C, 2 h	50	480 min	30.39 (Q_{max})	≈94	IPD	Langmuir	NR	(Umare et al., 2026)
BPBC	Banana peel	Pyrolysis 350 °C + acid washing	10–100	120 min	94.95 (Q_{max})	NR	PSO	Freundlich	NR	(Sayed et al., 2025)
Rosemary BC	Rosemary biomass	Pyrolysis 550 °C	NR	NR	28 (Q_{max})	NR	NR	Freundlich	NR	(Hmaied et al., 2025)
BCH	Peanut shell	Pyrolysis	20	60 min	8.67 (Q_{max})	95.36	PSO	Langmuir	5 cycles (>87%)	(Elmezayen et al., 2025)
NBCH	Peanut shell	N-doped + KOH activation	35	120 min	21.32 (Q_{max})	98.55	PSO, Elovich	Langmuir, Temkin	5 cycles (>90%)	(Elmezayen et al., 2025)

PTGA BC	*Torreya grandis* aril	Pyrolysis, non-activated	≤300	240 min	287.7 (Q_{max})	97.3	PSO	Langmuir	NR	(Si et al., 2025)
BDSS AC	Durian shells and seeds	Pyrolysis 500 °C + hydrothermal	50–500	60 min	136.99 (Q_{max})	94–97	PSO	Langmuir	3 cycles (53.7%)	(Huong et al., 2025)
KOH-AC	Rice straw residue	KOH activation, 800 °C	100–600	160 min	222 (Q_{max})	>95	PSO	Langmuir	3 cycles (loss)	(Wahyu et al., 2025)

*NR- Not reported

4.8 Proposed MB adsorption mechanism

The adsorption of MB onto the food waste-derived BC is governed by a combination of surface chemical interactions and structural features, as supported by kinetic, isotherm, pH-dependent, temperature-dependent, and spectroscopic analyses. The proposed adsorption pathways of MB onto food waste-derived BC are summarized schematically in Fig. 4.13, illustrating the combined roles of electrostatic attraction, hydrogen bonding, and π–π interactions. The collective evidence indicates that adsorption proceeds predominantly through chemisorption on a heterogeneous BC surface rather than simple physical uptake.

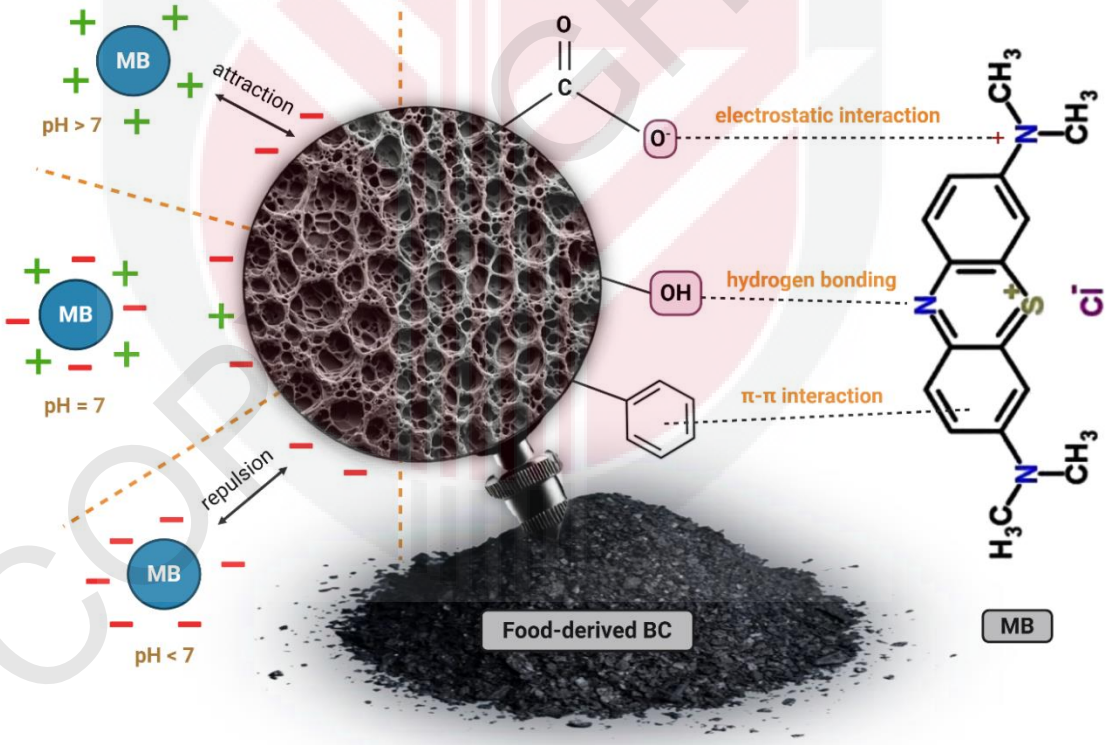

Fig. 4.14. Schematic illustration of the proposed adsorption mechanisms of MB onto food waste-derived BC.

FTIR analysis reveals the presence of oxygen-containing functional groups, including hydroxyl, carbonyl, and residual C–O moieties, particularly for BC prepared at lower to intermediate carbonization temperatures. These functional groups provide active sites for MB binding through electrostatic attraction and hydrogen bonding. The progressive reduction of oxygenated groups with increasing carbonization temperature, coupled with enhanced aromaticity, suggests a shift toward interaction mechanisms dominated by π–π stacking between the aromatic rings of MB and the graphitic domains of BC. This mechanism is consistent with the higher adsorption capacity observed for BC produced at elevated temperatures.

The strong pH dependence of adsorption further clarifies the mechanism. Under alkaline conditions, deprotonation of surface functional groups increases the negative surface charge of BC, enhancing electrostatic attraction toward cationic MB molecules. The markedly lower adsorption efficiency at acidic pH arises from surface protonation and competition between MB and protons for active sites. These trends confirm that electrostatic interactions play a major role in MB uptake, particularly at favorable pH conditions.

Kinetic analysis provides additional mechanistic insight. The superior fit of the PSO model across all MB concentrations indicates that the adsorption rate is controlled by surface reactions involving valence forces rather than by external mass transfer alone. The applicability of the Elovich model further supports adsorption on an energetically heterogeneous surface, where high-energy sites are occupied first, followed by progressively weaker interactions as surface coverage increases. This behavior reflects the diverse chemical environments created by mixed food-waste feedstocks.

Isotherm analysis reinforces these conclusions. While the Langmuir model provides only moderate fitting, the Temkin model best describes the equilibrium data, indicating that adsorption energy decreases linearly with increasing surface coverage. This observation suggests strong adsorbate–adsorbent interactions and confirms that MB

adsorption is influenced by interaction energy effects rather than ideal monolayer formation. Such behavior is characteristic of systems governed by electrostatic attraction, π–π interactions, and surface complexation.

Thermodynamic evaluation shows that adsorption capacity increases with temperature, indicating an endothermic process. Elevated temperatures enhance MB molecular mobility and diffusion into BC pores and strengthen adsorbate–adsorbent interactions. This thermally favored behavior supports chemisorption rather than weak physisorption as the dominant mechanism.

Based on the integrated evidence, MB adsorption onto food-derived BC proceeds through a synergistic mechanism involving electrostatic attraction between deprotonated surface groups and cationic MB, π–π stacking between aromatic structures, hydrogen bonding with residual oxygen-containing groups, and surface complexation on heterogeneous active sites. The relative contribution of each mechanism depends on carbonization temperature, solution pH, and operating conditions, explaining the observed trends in adsorption performance and model fitting.

4.9 Cost analysis

The cost breakdown for laboratory-scale production of food waste-derived BC is presented in Table 4.4 and is quantified on a per-batch basis, yielding approximately 5 g of BC. The total production cost per batch is RM 4.74, reflecting contributions from raw materials, processing energy, water usage, and equipment depreciation.

Raw material cost is effectively zero. A total of 10.00 g of food waste-derived biomass was used as the BC precursor, with no purchase cost incurred. This eliminates feedstock expenditure, which often represents a significant cost component in biomass-derived adsorbents. Process-related costs amount to RM 3.44 per batch and

dominate the overall expenditure. Deionized water consumption contributes RM 2.00, based on 200 mL at RM 0.01 per mL, used solely for washing and cleaning steps. Carbonization accounts for RM 1.44, calculated from an electricity consumption of 6.0 kWh over 2 h of furnace operation at an electricity tariff of RM 0.24 per kWh. This confirms that energy usage during thermal treatment is the principal variable cost driver.

Equipment depreciation contributes RM 1.30 per batch, associated with the centrifuge and filtration setup used for adsorbent recovery. No specialized or high-cost instrumentation was required, limiting capital-related overheads. When normalized to product yield, the overall cost corresponds to approximately RM 2.07 per gram of BC. This value remains competitive relative to reported biomass-derived BC adsorbents, particularly those involving chemical activation or solvent-intensive processing routes.

Importantly, the table indicates strong scalability potential. Carbonizing larger quantities of food waste per batch would distribute the fixed energy and equipment depreciation costs over a higher BC yield, directly reducing the unit production cost. Bulk carbonization therefore represents a realistic pathway for cost reduction without modifying synthesis chemistry or adsorption performa

Table 4.4. Cost breakdown for laboratory-scale production of food waste-derived BC.

Item	Quantity (per batch)	Unit Cost (RM)	Total Cost (RM)	Notes
Raw Materials				
Food waste-derived biomass	10.0 g	0.00/g	0.00	Main BC source
Total Raw Material Cost			**0.00**	
Synthesis Process				
Deionized water	200 mL	0.01/mL	2.00	For washing adsorbent
Carbonization	3.0 kWh X 2 hours = 6.0 kWh	RM 0.24 per kWh*	1.44	Energy cost for box furnace operation
Total Process Cost			**3.44**	
Equipment Depreciation				
Centrifuge/filtration setup	-	-	1.30	Equipment for recovery and filtration
Total Equipment Cost			**1.30**	
Overall cost			**4.74**	Per batch (2.29 g yield)

Notes: *refer to the Sarawak Energy tariff rate.

CHAPTER 5

CONCLUSION AND FUTURE WORKS

5.1 Conclusion

This study confirms the effectiveness of food waste-derived BC for MB removal from aqueous systems and demonstrates that adsorption performance is governed by surface chemistry, structural evolution, and operating conditions. Among the prepared materials, BC produced at 700 °C exhibits the most favorable characteristics for adsorption, reflecting advanced carbonization and structural stabilization. FTIR analysis shows a reduction in labile oxygen-containing functional groups and an increase in aromatic carbon structures at higher carbonization temperature, which promotes stronger π–π interactions with MB. XRD patterns confirm the predominantly amorphous nature of BC, while FESEM images reveal well-developed porosity, surface roughness, and interconnected pore networks at 700 °C, all of which enhance accessibility of active sites. TGA further indicates improved thermal stability and higher fixed-carbon content for BC700, supporting its suitability for repeated adsorption cycles.

Adsorption efficiency increases systematically with BC dosage, with optimal performance observed at 50 mg due to increased availability of accessible adsorption sites. Solution pH exerts a dominant influence, with markedly enhanced MB uptake under alkaline conditions and maximum removal at pH 12.21. This behavior arises from electrostatic attraction between deprotonated BC surface sites and cationic MB, supported by hydrogen bonding and π–π interactions. Temperature positively influences adsorption, with higher capacities achieved at 45 °C, indicating an

endothermic process driven by enhanced molecular mobility and stronger adsorbate–adsorbent interactions.

Kinetic analysis shows that at lower MB concentrations, the good agreement with the Elovich model highlights the importance of surface heterogeneity and rapid adsorption on high-energy active sites. As the concentration increases, the PSO model provides a superior fit, demonstrating that chemisorption becomes the dominant rate-controlling mechanism due to increased interaction between MB molecules and functional groups on the BC surface. Equilibrium analysis reveals non-ideal adsorption behavior. While the Langmuir model provides capacity estimates, deviations from monolayer assumptions reflect surface heterogeneity. The Freundlich model confirms favorable adsorption, and the superior fit of the Temkin isotherm highlights interaction-controlled adsorption with decreasing adsorption energy as surface coverage increases.

Comparative assessment with reported BC-based adsorbents demonstrates that the food waste-derived BC developed in this study achieves competitive adsorption capacity and removal efficiency under milder synthesis and operating conditions, without chemical activation or surface modification. Cost analysis further shows that production (RM 0.95/g) is dominated by energy input, with negligible raw material cost and minimal consumables, supporting economic and environmental feasibility.

Overall, MB adsorption onto food waste-derived BC, particularly BC produced at 700 °C, proceeds via a chemisorption-dominated, multi-interaction mechanism on a heterogeneous surface involving electrostatic attraction, π–π stacking, and hydrogen bonding. The combination of moderate dosage, alkaline pH, and elevated temperature yields optimal performance. These findings position food waste-derived BC as a practical, low-cost, and scalable adsorbent for dye-contaminated wastewater treatment and provide a clear framework for future optimization and scale-up.

5.2 Future works

Future research should focus on advancing both the material design and practical deployment of food waste-derived BC for wastewater treatment. First, optimization of adsorbent preparation warrants further attention. Systematic variation of carbonization temperature, residence time, and precursor composition would enable fine control over pore architecture, surface area, and functional group distribution. In addition, targeted surface modification through mild acid or base treatment, heteroatom doping, or physical activation could be explored to enhance adsorption capacity and selectivity toward cationic dyes such as MB while preserving low-cost and sustainable processing.

Second, advanced characterization is needed to deepen structural and chemical understanding. High-resolution techniques such as transmission electron microscopy and atomic force microscopy would provide direct evidence of pore development, surface roughness, and nanoscale morphology. Complementary surface-sensitive analyses using X-ray photoelectron spectroscopy and Raman spectroscopy would clarify bonding states, defect density, and the specific role of oxygen-containing and aromatic functionalities in adsorption. Third, adsorption performance should be extended beyond model systems. Evaluation against a wider range of organic dyes and emerging contaminants would establish the versatility of the adsorbent. More importantly, testing under real wastewater conditions is essential to assess performance in complex matrices containing competing ions, natural organic matter, and fluctuating pH.

Finally, deeper mechanistic and applicability studies are required. Quantitative surface charge analysis using zeta potential measurements and in situ spectroscopic techniques would strengthen understanding of electrostatic, π–π, and surface complexation mechanisms. Long-term regeneration, repeated adsorption–desorption

cycling, and stability assessments should also be prioritized to determine operational lifetime and economic feasibility at larger scales.

References

Ahmad, A., Khan, N., Giri, B. S., Chowdhary, P., & Chaturvedi, P. (2020). Removal of methylene blue dye using rice husk, cow dung and sludge biochar: Characterization, application, and kinetic studies. *Bioresource Technology*, *306*, 123202. https://doi.org/10.1016/j.biortech.2020.123202

Beigmohammadi, F., Solgi, E., Besalatpour, A. A., & Soleimani, M. (2024). Immobilization of potentially toxic elements by grape waste biochar in contaminated soils. *Geoderma Regional*, *39*, e00900. https://doi.org/10.1016/j.geodrs.2024.e00900

Benamer-Oudih, S., Tahtat, D., Nacer Khodja, A., Mansouri, B., Mahlous, M., Guittoum, A. E., & Kebbouche Gana, S. (2023). Sorption behavior of chitosan nanoparticles for single and binary removal of cationic and anionic dyes from aqueous solution. *Environmental Science and Pollution Research*, *31*(28), 39976–39993. https://doi.org/10.1007/s11356-023-27907-0

Chatzimichailidou, S., Xanthopoulou, M., Tolkou, A. K., & Katsoyiannis, I. A. (2023). Biochar Derived from Rice by-Products for Arsenic and Chromium Removal by Adsorption: A Review. *Journal of Composites Science*, *7*(2), 59. https://doi.org/10.3390/jcs7020059

Chen, L.-Y., Meng, X.-G., Yu, W.-W., Zhang, Y.-L., Gan, Z.-Y., & Yang, C. (2023). Efficient separation of cellulose from bamboo by organic alkali. *Cellulose*, *30*(3), 1369–1379. https://doi.org/10.1007/s10570-022-04969-w

Chen, W.-H., Lin, B.-J., Lin, Y.-Y., Chu, Y.-S., Ubando, A. T., Show, P. L., Ong, H. C., Chang, J.-S., Ho, S.-H., Culaba, A. B., Pétrissans, A., & Pétrissans, M. (2021). Progress in biomass torrefaction: Principles, applications and challenges. *Progress in Energy and Combustion Science*, *82*, 100887. https://doi.org/10.1016/j.pecs.2020.100887

Chutani, A., Verma, N., & Kumar, V. (2026). Valorization of manila tamarind seed coat waste biomass for dye removal. *Sustainable Chemistry One World*, *9*, 100160. https://doi.org/10.1016/j.scowo.2025.100160

Dong, X., Chu, Y., Tong, Z., Sun, M., Meng, D., Yi, X., Gao, T., Wang, M., & Duan, J. (2024). Mechanisms of adsorption and functionalization of biochar for pesticides: A review. *Ecotoxicology and Environmental Safety*, *272*, 116019. https://doi.org/10.1016/j.ecoenv.2024.116019

Ebrahimzadeh, F., & Akbari, A. (2025). Investigation the adsorption mechanisms, chemical resistance and mechanical strength of the synthesized chitosan/activated carbon composite in methylene blue removal. *Scientific Reports*, *15*(1), 37820. https://doi.org/10.1038/s41598-025-21734-8

El Jery, A., Alawamleh, H. S. K., Sami, M. H., Abbas, H. A., Sammen, S. Sh., Ahsan, A., Imteaz, M. A., Shanableh, A., Shafiquzzaman, Md., Osman, H., & Al-Ansari, N. (2024). Isotherms, kinetics and thermodynamic mechanism of methylene blue dye adsorption on synthesized activated carbon. *Scientific Reports*, *14*(1), 970. https://doi.org/10.1038/s41598-023-50937-0

Elmezayen, M. R., Elhusseiny, A. F., Refaat, H. M., Hussein, S. M., Elsayed, E. H., & El-Dissouky, A. (2025). Insight into two sustainable, efficient, low-cost adsorbents derived biochar for aqueous removal of industrial dye. *Journal of Molecular Liquids*, *438*, 128724. https://doi.org/10.1016/j.molliq.2025.128724

Fan, S., Wang, Y., Wang, Z., Tang, J., Tang, J., & Li, X. (2017). Removal of methylene blue from aqueous solution by sewage sludge-derived biochar: Adsorption kinetics, equilibrium, thermodynamics and mechanism. *Journal of Environmental Chemical Engineering*, *5*(1), 601–611. https://doi.org/10.1016/j.jece.2016.12.019

Foo, K. Y., & Hameed, B. H. (2010). Insights into the modeling of adsorption isotherm systems. *Chemical Engineering Journal*, *156*(1), 2–10. https://doi.org/10.1016/j.cej.2009.09.013

Gao, Y., Yue, Q., Gao, B., & Li, A. (2020). Insight into activated carbon from different kinds of chemical activating agents: A review. *Science of The Total Environment*, *746*, 141094. https://doi.org/10.1016/j.scitotenv.2020.141094

Gayathiri, M., Pulingam, T., Lee, K. T., Mohd Din, A. T., Kosugi, A., & Sudesh, K. (2023). Sustainable oil palm trunk fibre based activated carbon for the adsorption of methylene blue. *Scientific Reports*, *13*(1), 22137. https://doi.org/10.1038/s41598-023-49079-0

G.P. Avinash, S. Karthick Raja Namasivayam, Kavisri, M., & Meivelu Moovendhan. (2025). Sustainable adsorption of methylene blue by biocompatible agro waste biomass: optimization, kinetic isotherms, and ecotoxicity evaluation. *Biomass Conversion and Biorefinery*, *15*(11), 16871–16890. https://doi.org/10.1007/s13399-024-06284-9

Guo, J., Liang, J., Zhang, T., Li, X., Wang, L., Li, Y., & Feng, X. (2024). *Effect of Modification on the Adsorption Performance of Mb by Rice Husk Biochar*. https://doi.org/10.2139/ssrn.4699476

Handayati, Y., & Widyanata, C. (2024). Effective food waste management model for the sustainable agricultural food supply chain. *Scientific Reports*, *14*(1), 10290. https://doi.org/10.1038/s41598-024-59482-w

Haris, M., Hamid, Y., Usman, M., Wang, L., Saleem, A., Su, F., Guo, J., & Li, Y. (2021). Crop-residues derived biochar: Synthesis, properties, characterization and application for the removal of trace elements in soils. *Journal of Hazardous Materials*, *416*, 126212. https://doi.org/10.1016/j.jhazmat.2021.126212

Hmaied, A., Trabelsi, A. B. H., Lachaal, F., Negro, S., & Hammecker, C. (2025). Biochars Derived from Diverse Local Tunisian Feedstocks for Environmental Remediation: Physicochemical Properties and Adsorption Behaviour. *Land*, *14*(11), 2224. https://doi.org/10.3390/land14112224

Ho, Y. S., & McKay, G. (1999). Pseudo-second order model for sorption processes. *Process Biochemistry*, *34*(5), 451–465. https://doi.org/10.1016/S0032-9592(98)00112-5

Hou, R., Zhang, J., Fu, Q., Li, T., Gao, S., Wang, R., Zhao, S., & Zhu, B. (2024). The boom era of emerging contaminants: A review of remediating agricultural soils by biochar. *Science of The Total Environment*, *931*, 172899. https://doi.org/10.1016/j.scitotenv.2024.172899

Huong, D. T., Ngan, N. N. P., Anh, D. T. T., Vinh, N. D., & Xuan, V. T. (2025). Durian peel–seed biochar for efficient methylene blue removal from water: synthesis, characterization, and adsorption performance. *RSC Advances*, *15*(40), 33726–33749. https://doi.org/10.1039/D5RA05313G

Karce, H. E., Boumessaidia, S., Bahloul, A., Lal, B., Saravanan, A., Ouakouak, A., Hosseini-Bandegharaei, A., Sridevi, C., & Prakash, C. (2025a). Efficient removal of methylene blue by a biochar from neem tree shell wastes using adsorption technology. *Biomass Conversion and Biorefinery*, *15*(9), 13559–13574. https://doi.org/10.1007/s13399-024-06072-5

Karce, H. E., Boumessaidia, S., Bahloul, A., Lal, B., Saravanan, A., Ouakouak, A., Hosseini-Bandegharaei, A., Sridevi, C., & Prakash, C. (2025b). Efficient removal of methylene blue by a biochar from neem tree shell wastes using adsorption technology. *Biomass Conversion and Biorefinery*, *15*(9), 13559–13574. https://doi.org/10.1007/s13399-024-06072-5

Kataya, G., Issa, M., Badran, A., Cornu, D., Bechelany, M., Jellali, S., Jeguirim, M., & Hijazi, A. (2025). Dynamic removal of methylene blue and methyl orange from water using biochar derived from kitchen waste. *Scientific Reports*, *15*(1), 29907. https://doi.org/10.1038/s41598-025-14133-6

Khan, I., Saeed, K., Zekker, I., Zhang, B., Hendi, A. H., Ahmad, A., Ahmad, S., Zada, N., Ahmad, H., Shah, L. A., Shah, T., & Khan, I. (2022). Review on Methylene Blue: Its Properties, Uses, Toxicity and Photodegradation. *Water*, *14*(2), 242. https://doi.org/10.3390/w14020242

Kim, D., Yoshikawa, K., & Park, K. (2015). Characteristics of Biochar Obtained by Hydrothermal Carbonization of Cellulose for Renewable Energy. *Energies*, *8*(12), 14040–14048. https://doi.org/10.3390/en81212412

Krysanova, K., Krylova, A., Kulikova, M., Kulikov, A., & Rusakova, O. (2022). Biochar characteristics produced via hydrothermal carbonization and torrefaction of peat and sawdust. *Fuel*, *328*, 125220. https://doi.org/10.1016/j.fuel.2022.125220

Kuang, Y., Zhang, X., & Zhou, S. (2020). Adsorption of Methylene Blue in Water onto Activated Carbon by Surfactant Modification. *Water*, *12*(2), 587. https://doi.org/10.3390/w12020587

Kujawska, J., & Wasag, H. (2021). Biochar: a low-cost adsorbent of Methylene Blue from aqueous solutions. *Journal of Physics: Conference Series*, *1736*(1), 012002. https://doi.org/10.1088/1742-6596/1736/1/012002

Kumari, R., Singh, A., Sharma, R., & Malaviya, P. (2024). Conversion of food waste into energy and value-added products: a review. *Environmental Chemistry Letters*, *22*(4), 1759–1790. https://doi.org/10.1007/s10311-024-01742-2

Li, D., Li, C., Qiu, L., Li, B., Jiang, Y., Liang, J., Zhang, S., Tang, Y., Wang, D., Leng, C., & Hu, X. (2024). Exchange of organics with homogenous volatiles shapes

nature of biochar of varied aspects. *Materials Today Sustainability*, *25*, 100655. https://doi.org/10.1016/j.mtsust.2023.100655

Li, D., Liu, C., Liu, Y., Chen, X., Wu, W., Li, F., Tian, J., & Dang, Z. (2022). Tannic acid as an eco-friendly natural passivator for the inhibition of pyrite oxidation to prevent acid mine drainage at the source. *Applied Surface Science*, *591*, 153172. https://doi.org/10.1016/j.apsusc.2022.153172

Li, H., Kong, J., Zhang, H., Gao, J., Fang, Y., Shi, J., Ge, T., Fang, T., Shi, Y., Zhang, R., Zhang, N., Dong, X., Zhang, Y., & Li, H. (2023). Mechanisms and adsorption capacities of ball milled biomass fly ash/biochar composites for the adsorption of methylene blue dye from aqueous solution. *Journal of Water Process Engineering*, *53*, 103713. https://doi.org/10.1016/j.jwpe.2023.103713

Li, Z., Zheng, Z., Li, H., Xu, D., Li, X., Xiang, L., & Tu, S. (2023). Review on Rice Husk Biochar as an Adsorbent for Soil and Water Remediation. *Plants*, *12*(7), 1524. https://doi.org/10.3390/plants12071524

Liu, Z., Niu, W., Chu, H., Zhou, T., & Niu, Z. (2018). Effect of the Carbonization Temperature on the Properties of Biochar Produced from the Pyrolysis of Crop Residues. *BioResources*, *13*(2). https://doi.org/10.15376/biores.13.2.3429-3446

Loc Ton-That, Hoang-Dung Pham, Thi-Ngoc-Linh Huynh, Bich-Ngoc Duong, Thi-Thuy Luu, Duy-Khoi Nguyen, Ngoc-An Nguyen, Thien-Hoang Ho, Van-Hien Pham, & Van-Phuc Dinh. (2023). Adsorption of methylene blue from aqueous solution by biochar prepared from jackfruit peel: isotherm model studies. *Vietnam Journal of Catalysis and Adsorption*, *12*(1), 1–7. https://doi.org/10.51316/jca.2023.001

Louros, V. L., Silva, V., Silva, C. P., Calisto, V., Otero, M., Esteves, V. I., Freitas, R., & Lima, D. L. D. (2022). Sulfadiazine's photodegradation using a novel magnetic and reusable carbon based photocatalyst: Photocatalytic efficiency and toxic

impacts to marine bivalves. *Journal of Environmental Management*, *313*, 115030. https://doi.org/10.1016/j.jenvman.2022.115030

Lu, Y., Liu, Y., Li, C., Liu, H., Liu, H., Tang, Y., Tang, C., Wang, A., & Wang, C. (2022a). Adsorption Characteristics and Mechanism of Methylene Blue in Water by NaOH-Modified Areca Residue Biochar. *Processes*, *10*(12), 2729. https://doi.org/10.3390/pr10122729

Lu, Y., Liu, Y., Li, C., Liu, H., Liu, H., Tang, Y., Tang, C., Wang, A., & Wang, C. (2022b). Adsorption Characteristics and Mechanism of Methylene Blue in Water by NaOH-Modified Areca Residue Biochar. *Processes*, *10*(12), 2729. https://doi.org/10.3390/pr10122729

Manyà, J. J. (2012). Pyrolysis for Biochar Purposes: A Review to Establish Current Knowledge Gaps and Research Needs. *Environmental Science & Technology*, *46*(15), 7939–7954. https://doi.org/10.1021/es301029g

Meftah, K., Meftah, S., Lamkhanter, H., Touil, S., & Abid, A. (2024). Study of Methylene Blue dye adsorption onto biochar derived from Austrocylindropuntia subulata plant. *IOP Conference Series: Earth and Environmental Science*, *1398*(1), 012006. https://doi.org/10.1088/1755-1315/1398/1/012006

Meng, F., Zhang, J., Liu, Q., Wang, D., Li, F., & Wang, J. (2024a). Biochar derived from biogas fermentation residue with enhanced absorption property suitable for efficient absorption of methylene blue in aqueous. *Colloids and Surfaces A: Physicochemical and Engineering Aspects*, *703*, 135407. https://doi.org/10.1016/j.colsurfa.2024.135407

Meng, F., Zhang, J., Liu, Q., Wang, D., Li, F., & Wang, J. (2024b). Biochar derived from biogas fermentation residue with enhanced absorption property suitable for efficient absorption of methylene blue in aqueous. *Colloids and Surfaces A:*

Physicochemical and Engineering Aspects, *703*, 135407. https://doi.org/10.1016/j.colsurfa.2024.135407

Moeinfar, M., Ghiasvand, A., & Khaleghi, E. (2024). Chemical bonding of cross-linked glutaraldehyde/chitosan on the surface of a titanium wire to prepare a robust biocompatible SPME fiber for analysis of phytohormones in plants. *Food Chemistry*, *449*, 139168. https://doi.org/10.1016/j.foodchem.2024.139168

Moureen, A., Waqas, M., Khan, N., Jabeen, F., Magazzino, C., Jamila, N., & Beyazli, D. (2024). Untapped potential of food waste derived biochar for the removal of heavy metals from wastewater. *Chemosphere*, *356*, 141932. https://doi.org/10.1016/j.chemosphere.2024.141932

Mozaffari Majd, M., Kordzadeh-Kermani, V., Ghalandari, V., Askari, A., & Sillanpää, M. (2022). Adsorption isotherm models: A comprehensive and systematic review (2010−2020). *Science of The Total Environment*, *812*, 151334. https://doi.org/10.1016/j.scitotenv.2021.151334

Musa, A., Sani, B. S., Ibrahim, F. B., & Giwa, A. (2025). Comparative Analysis of the Adsorption of Methylene Blue Using Magnetised and Non-Magnetised Coconut Shell Biochar. *Uniosun Journal of Engineering and Environmental Sciences*, *1*(2). https://doi.org/10.36108/ujees/9102.10.0250

Muteeb, G., Ansari, K., Eyvaz, M., Farhan, M., Aatif, M., Agrawal, D., Oirdi, M. El, & Dehghani, M. H. (2025). Removal of methylene blue (MB) dye from water and wastewater using acid-activated chicken bone in a batch adsorption process. *Scientific Reports*, *15*(1), 23098. https://doi.org/10.1038/s41598-025-08341-3

Nan, H., Yin, J., Yang, F., Luo, Y., Zhao, L., & Cao, X. (2021). Pyrolysis temperature-dependent carbon retention and stability of biochar with participation of calcium: Implications to carbon sequestration. *Environmental Pollution*, *287*, 117566. https://doi.org/10.1016/j.envpol.2021.117566

Olupot, P. W., Wakatuntu, J., Turyasingura, M., Jjagwe, J., Menya, E., & Okure, M. (2024). Optimization of heavy metal removal by activated carbon obtained as a co-product from fast pyrolysis of rice husks. *Results in Materials*, *21*, 100545. https://doi.org/10.1016/j.rinma.2024.100545

Ortega-Toro, R., Villabona-Ortíz, Á., Tejada-Tovar, C., Herrera-Barros, A., & Cabrales-Sanjuan, D. (2023). Use of Sawdust (Aspidosperma polyneuron) in the Preparation of a Biocarbon-Type Adsorbent Material for Its Potential Use in the Elimination of Cationic Contaminants in Wastewater. *Water*, *15*(21), 3868. https://doi.org/10.3390/w15213868

Periyasamy, A. P. (2024). Recent Advances in the Remediation of Textile-Dye-Containing Wastewater: Prioritizing Human Health and Sustainable Wastewater Treatment. *Sustainability*, *16*(2), 495. https://doi.org/10.3390/su16020495

Qing, M., Huang, S., Liu, L., Chen, Y., Zhang, L., Liu, W., Yin, Y., He, J., & Xiang, J. (2024). Construction of a food waste biochar model and determination of contaminant adsorption sites: Combining experimental characterisation with quantum chemical calculations. *Journal of Molecular Structure*, *1310*, 138273. https://doi.org/10.1016/j.molstruc.2024.138273

Řimnáčová, D., Bičáková, O., Moško, J., Straka, P., & Čimová, N. (2024). The effect of carbonization temperature on textural properties of sewage sludge-derived biochars as potential adsorbents. *Journal of Environmental Management*, *359*, 120947. https://doi.org/10.1016/j.jenvman.2024.120947

Sahu, S., Pahi, S., Sahu, J. K., Sahu, U. K., & Patel, R. K. (2020). Kendu (Diospyros melanoxylon Roxb) fruit peel activated carbon—an efficient bioadsorbent for methylene blue dye: equilibrium, kinetic, and thermodynamic study. *Environmental Science and Pollution Research*, *27*(18), 22579–22592. https://doi.org/10.1007/s11356-020-08561-2

Sarwar, A., Ali, M., Khoja, A. H., Nawar, A., Waqas, A., Liaquat, R., Naqvi, S. R., & Asjid, M. (2021). Synthesis and characterization of biomass-derived surface-modified activated carbon for enhanced CO2 adsorption. *Journal of CO2 Utilization*, *46*, 101476. https://doi.org/10.1016/j.jcou.2021.101476

Satyam, S., & Patra, S. (2024). Innovations and challenges in adsorption-based wastewater remediation: A comprehensive review. *Heliyon*, *10*(9), e29573. https://doi.org/10.1016/j.heliyon.2024.e29573

Sayed, A., Behalo, M., Feteha, A., Younis, A., Keshawy, M., Yousry, R., & Abdel-Raouf, M. E. (2025). Unveiling the removal performance of banana peel biochar and rice husk nanoparticles for crystal violet and methylene blue dyes from aqueous media. *Discover Environment*, *3*(1), 143. https://doi.org/10.1007/s44274-025-00354-z

Scherhaufer, S., Moates, G., Hartikainen, H., Waldron, K., & Obersteiner, G. (2018). Environmental impacts of food waste in Europe. *Waste Management*, *77*, 98–113. https://doi.org/10.1016/j.wasman.2018.04.038

Shanmugam, H., Raghavan, V., Rajagopal, R., Goyette, B., Lyu, L., Zhou, S., & An, C. (2024). Evaluating Sustainable Practices for Managing Residue Derived from Wheat Straw. *Bioengineering*, *11*(6), 554. https://doi.org/10.3390/bioengineering11060554

Shao, Y., Li, C., Fan, M., Gao, G., Jiang, Y., Sun, K., Zhang, L., Zhang, S., Xu, L., & Hu, X. (2023a). Torrefaction and hydrothermal carbonization pretreatments of rice impact nature of biochar from subsequent pyrolysis. *Industrial Crops and Products*, *205*, 117515. https://doi.org/10.1016/j.indcrop.2023.117515

Shao, Y., Li, C., Fan, M., Gao, G., Jiang, Y., Sun, K., Zhang, L., Zhang, S., Xu, L., & Hu, X. (2023b). Torrefaction and hydrothermal carbonization pretreatments of rice

impact nature of biochar from subsequent pyrolysis. *Industrial Crops and Products*, *205*, 117515. https://doi.org/10.1016/j.indcrop.2023.117515

Shao, Z., Zhao, Y., Wang, S., Xie, L., Zhang, L., Xu, K., & Chai, X. (2025). Effects and mechanisms of Fe/N co-doped magnetic biochar for efficient removal of single and multiple dye. *Colloids and Surfaces A: Physicochemical and Engineering Aspects*, *704*, 135505. https://doi.org/10.1016/j.colsurfa.2024.135505

Si, W., Xia, S., Su, M., Shi, C., & Zhang, T. (2025). Studies of the adsorption properties of methylene blue onto the low-cost Torreya grandis aril biochar without activation. *Desalination and Water Treatment*, *324*, 101562. https://doi.org/10.1016/j.dwt.2025.101562

Takele, T., Angassa, K., Abewaa, M., Kebede, A. M., & Tessema, I. (2025). Adsorption of methylene blue from textile industrial wastewater using activated carbon developed from H3PO4-activated khat stem waste. *Biomass Conversion and Biorefinery*, *15*(3), 4085–4108. https://doi.org/10.1007/s13399-023-05245-y

Tolkou, A. K., Tsoutsa, E. K., Kyzas, G. Z., & Katsoyiannis, I. A. (2024). Sustainable use of low-cost adsorbents prepared from waste fruit peels for the removal of selected reactive and basic dyes found in wastewaters. *Environmental Science and Pollution Research*, *31*(10), 14662–14689. https://doi.org/10.1007/s11356-024-31868-3

Tripathi, N., Rodriguez Uribe, A., Weldekidan, H., Misra, M., & Mohanty, A. K. (2022). Upcycling of waste jute biomass to advanced biocarbon materials: the effect of pyrolysis temperature on their physicochemical and electrical properties. *Materials Advances*, *3*(24), 9071–9082. https://doi.org/10.1039/D2MA00678B

Umare, S., Thawait, A. K., & Dhawane, S. H. (2026). Development and optimization of sustainable activated biochar from waste pigeon pea stalks for efficient adsorptive

removal of methylene blue from water. *Biomass and Bioenergy*, *204*, 108385. https://doi.org/10.1016/j.biombioe.2025.108385

Vafakish, B., Babaei-Ghazvini, A., & Acharya, B. (2025). Unraveling the mechanisms of methylene blue adsorption onto biochar: a robust and sustainable approach for water remediation. *International Journal of Environmental Science and Technology*, *22*(8), 7053–7064. https://doi.org/10.1007/s13762-024-06111-8

Vigdorowitsch, M., Pchelintsev, A., Tsygankova, L., & Tanygina, E. (2021). Freundlich Isotherm: An Adsorption Model Complete Framework. *Applied Sciences*, *11*(17), 8078. https://doi.org/10.3390/app11178078

Vojnović, B., Cetina, M., Franjković, P., & Sutlović, A. (2022). Influence of Initial pH Value on the Adsorption of Reactive Black 5 Dye on Powdered Activated Carbon: Kinetics, Mechanisms, and Thermodynamics. *Molecules*, *27*(4), 1349. https://doi.org/10.3390/molecules27041349

Wahyu, M. E., Damayanti, D., & Wu, H. S. (2025). Production, Characterization, and Application of KOH-Activated Biochar from Rice Straw for Azo Dye Adsorption. *Biomass*, *5*(3), 40. https://doi.org/10.3390/biomass5030040

Wang, J., Tan, Y., Yang, H., Zhan, L., Sun, G., & Luo, L. (2023). On the adsorption characteristics and mechanism of methylene blue by ball mill modified biochar. *Scientific Reports*, *13*(1), 21174. https://doi.org/10.1038/s41598-023-48373-1

Wang, K., Peng, N., Zhang, D., Zhou, H., Gu, J., Huang, J., Liu, C., Chen, Y., Liu, Y., & Sun, J. (2023). Efficient removal of methylene blue using Ca(OH)2 modified biochar derived from rice straw. *Environmental Technology & Innovation*, *31*, 103145. https://doi.org/10.1016/j.eti.2023.103145

Wu, S., Li, Y., Wang, T., Li, H., Wang, X., Ma, L., Zhang, N., Yue, P., & Li, Y. (2023). Design and synthesis of dual functional porphyrin-based COFs as highly selective

adsorbent and photocatalyst. *Chemical Engineering Journal*, *470*, 144135. https://doi.org/10.1016/j.cej.2023.144135

Xie, Y., Wang, L., Li, H., Westholm, L. J., Carvalho, L., Thorin, E., Yu, Z., Yu, X., & Skreiberg, Ø. (2022). A critical review on production, modification and utilization of biochar. *Journal of Analytical and Applied Pyrolysis*, *161*, 105405. https://doi.org/10.1016/j.jaap.2021.105405

Yang, C., Wu, H., Cai, M., Li, Y., Guo, C., Han, Y., Zhang, Y., & Song, B. (2023). Valorization of food waste digestate to ash and biochar composites for high performance adsorption of methylene blue. *Journal of Cleaner Production*, *397*, 136612. https://doi.org/10.1016/j.jclepro.2023.136612

Zakaria, M. R., Ahmad Farid, M. A., Andou, Y., Ramli, I., & Hassan, M. A. (2023). Production of biochar and activated carbon from oil palm biomass: Current status, prospects, and challenges. *Industrial Crops and Products*, *199*, 116767. https://doi.org/10.1016/j.indcrop.2023.116767

Zamri, M. Z. A., Yahya, N. Y., Ramli, R. S., Ngadi, N., & Widia, M. (2019). Characterization of Banana peels waste adsorbent for preliminary study of methylene blue removal from aqueous solution. *IOP Conference Series: Materials Science and Engineering*, *697*(1), 012033. https://doi.org/10.1088/1757-899X/697/1/012033

Zhu, Y., Yi, B., Yuan, Q., Wu, Y., Wang, M., & Yan, S. (2018). Removal of methylene blue from aqueous solution by cattle manure-derived low temperature biochar. *RSC Advances*, *8*(36), 19917–19929. https://doi.org/10.1039/C8RA03018A

APPENDIX

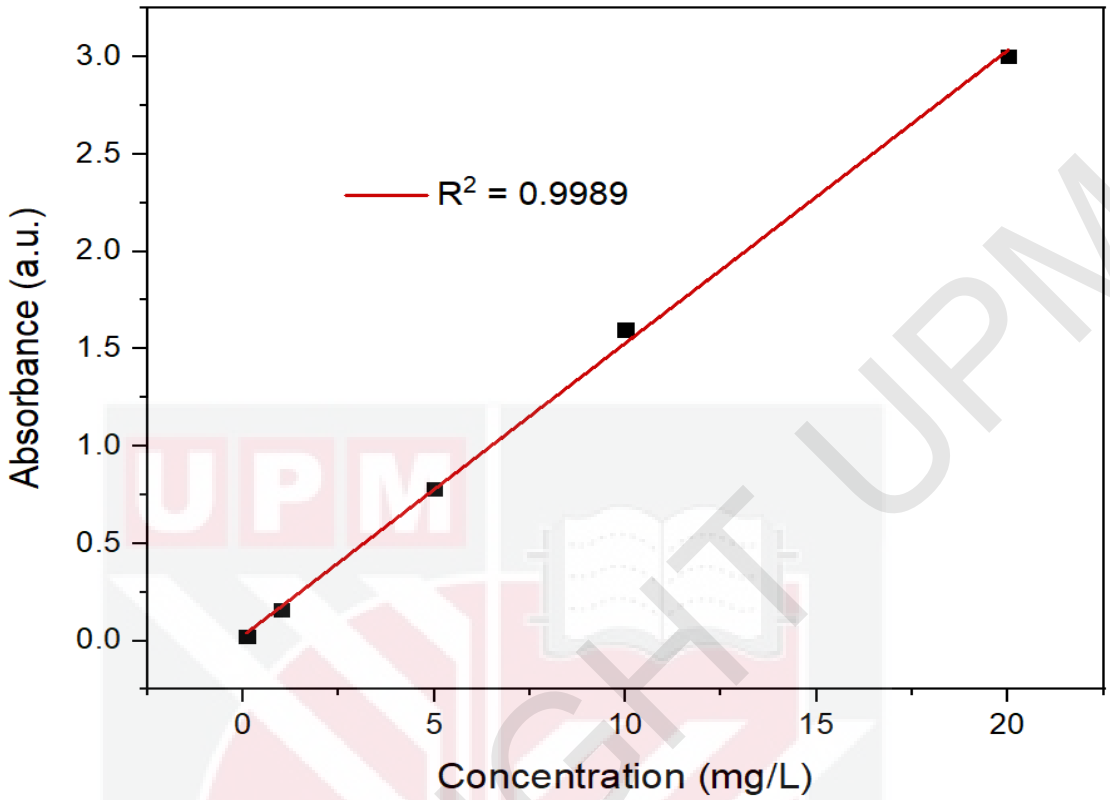

Fig. S1 Calibration curve of MB at 664 nm.

BIOGRAPHY OF THE STUDENT

Anisah Sahimi is a motivated and detail-oriented individual with a strong academic foundation in industrial chemistry. She is currently completing a Bachelor of Science (Hons.) in Industrial Chemistry at Universiti Putra Malaysia Sarawak (UPMS), where she has developed a solid understanding of chemical processes, materials, and analytical techniques. Prior to her undergraduate studies, Anisah completed her Matriculation in Pure Science at Pahang Matriculation College, which provided a strong scientific foundation and nurtured her interest in chemistry and sustainable technologies.

During her undergraduate program, Anisah has conducted research on Preparation of food waste – derived biochar for adsorption of methylene blue, focusing on material synthesis, optimization, and understanding adsorption mechanisms. Her work demonstrates proficiency in laboratory techniques such as FTIR, XRD, UV-Vis spectroscopy, and adsorption kinetics analysis, as well as strong analytical and problem-solving skills.

Anisah's hands-on experience in synthesizing and characterizing advanced materials, combined with her ability to interpret experimental results, has prepared her for a future career in industrial and environmental chemistry. She is passionate about developing innovative and sustainable solutions for pollution control, water treatment, and renewable energy applications. Anisah's academic dedication, research experience, and analytical mindset highlight her potential to contribute meaningfully to the field of industrial chemistry.